228 (2023) 211955

Contents lists available at ScienceDirect

Geoenergy Science and Engineering

journal homepage: www.sciencedirect.com/journal/geoenergy-science-and-engineering

Delineation and quantification of effective source rocks using 3D geological modeling in a lacustrine basin

Bang Zeng [a], Meijun Li [a,b,*], Yang Shi [c], Xin Wang [a], Hao Guo [c], Junhao Ren [a], Xi He [a]

[a] State Key Laboratory of Petroleum Resources and Prospecting, College of Geosciences, China University of Petroleum (Beijing), Beijing, 102249, China
[b] State Key Laboratory of Petroleum Resources and Prospecting, Faculty of Petroleum, China University of Petroleum-Beijing at Karamay, Karamay, 834000, China
[c] Southern Oil Exploration and Development Company, PetroChina, Haikou, 570216, China

ARTICLE INFO

Keywords:
Lacustrine basin
Effective source rocks
Hydrocarbon generation and expulsion potential
3D geological modeling

ABSTRACT

The identification and quantification of effective source rocks are critical for hydrocarbon exploration, but traditional methods have limitations in lacustrine basins due to their complexity and heterogeneity. For example, geochemical analysis is constrained by the number and distribution of samples, well logging methods can only reflect local information, and seismic inversion methods are limited by the quality and resolution of data. We propose a geological modeling approach that combines geophysical techniques and geological and geochemical data to delineate effective source rocks and quantify hydrocarbon resource potential. The workflow includes mudstone classification, geochemical data analysis, building predictive models, constructing 3D geological models, filtering effective source rocks, and basin simulation. Taking the Fushan Depression, South China Sea, as an example, we estimate the total volume of effective oil source rocks at 323.48 km^3 and effective gas source rocks at 67.43 km^3, and identify favorable areas for conventional and unconventional hydrocarbon exploration. The results demonstrate that our proposed approach enables precise delineation of the spatial distribution of effective hydrocarbon source rocks and quantification of their potential for hydrocarbon generation and expulsion. Our study constitutes a reference case for assessing effective source rocks in other lacustrine basins due to the successful integration of multiple available of data and its practical applications.

1. Introduction

Effective source rock refers to rock that contains a significant amount of organic matter and expels hydrocarbons during geological evolution (Hunt, 1979; Tissot and Welte, 1984; Pang et al., 2005). These active source rocks are a crucial factor in the occurrence of hydrocarbon accumulation (Magoon, 2004). Thus, accurately determining their spatial distribution and quantity is critical for locating hydrocarbon exploration objectives. Conventional source rock investigation mainly involves outcrop observation, microscopic observation, numerous geochemical experiments, and statistical analysis to assess the hydrocarbon generation potential, paleoenvironment, and distribution range of effective source rocks (Peters, 1986; Hunt, 1996; Sheikh et al., 2016; Zheng et al., 2019; Mansour et al., 2023; Hakimi et al., 2023). The most commonly used techniques for calculating geochemical characteristic isoline values are the weighted average method and the interpolation method (Peters et al., 2006; Zhu et al., 2021). However, the limited quantity and distribution of available samples restrict the precision of these studies, making conventional methods insufficient for directly guiding oil and gas exploration particularly in regions with moderate to low exploration levels. While continuous logging curves have been used to estimate the total organic carbon (TOC), volatile hydrocarbon (S_1), and remaining hydrocarbon generation potential (S_2) in individual wells, this approach only provides local information, and the regional and spatial heterogeneity of effective source rock remains difficult to depict. (Schmoker, 1979; Fertl and Chilingar, 1988; Passey et al., 1990; Mahmoud et al., 2017; Wang et al., 2019). Although some geophysicists have attempted to identify effective source rocks on seismic data by delineating characteristic acoustic parameters and related seismic response of organic-rich mudstones, this method is limited by the high-quality requirements and relatively low resolution of seismic data in many cases. (Løseth et al., 2011; Ogiesba and Hammes, 2014; Sahoo et al., 2021). Moreover ~~Morever~~, effective source rocks are also considered unconventional economic reservoirs, requiring greater resolution and accuracy in their description. Therefore, there is a pressing need to develop a method that can precisely describe the spatial

* Corresponding author. State Key Laboratory of Petroleum Resources and Prospecting, College of Geosciences, China University of Petroleum Beijing, China.
E-mail address: meijunli@cup.edu.cn (M. Li).

https://doi.org/10.1016/j.geoen.2023.211955
Received 12 April 2023; Received in revised form 27 May 2023; Accepted 29 May 2023
Available online 7 June 2023

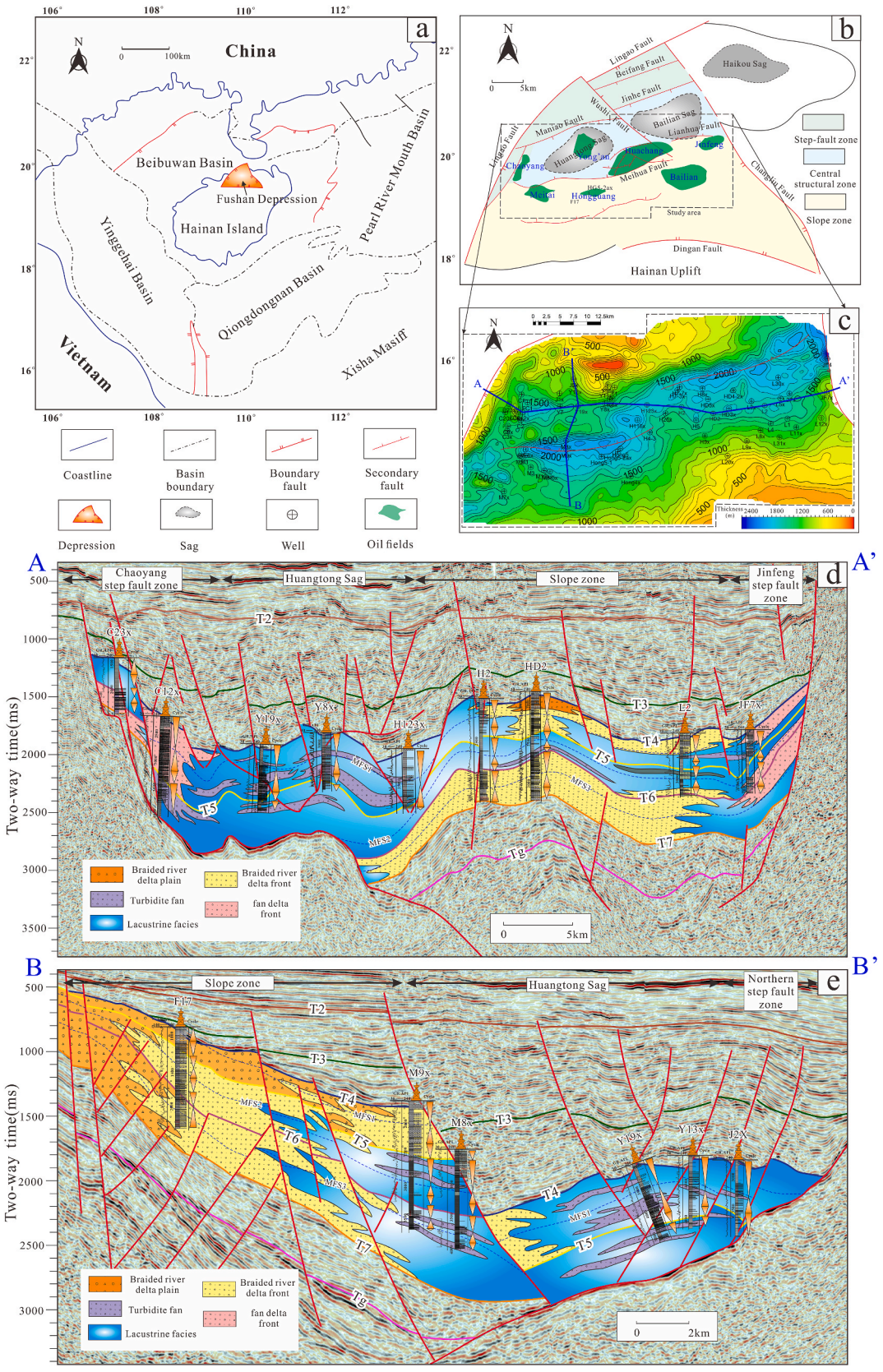

Fig. 1. (a) Location of the Fushan Depression (Liu et al., 2014). (b) Division of structural units in the Fushan Depression (Gan et al., 2020). (c) The contour map showing strata thickness of the Liushagang Formation. (d) and (e) The sections showing the sequence stratigraphic and sedimentary evolutions of the Liushagang Formation. MFS: maximum flooding surface.

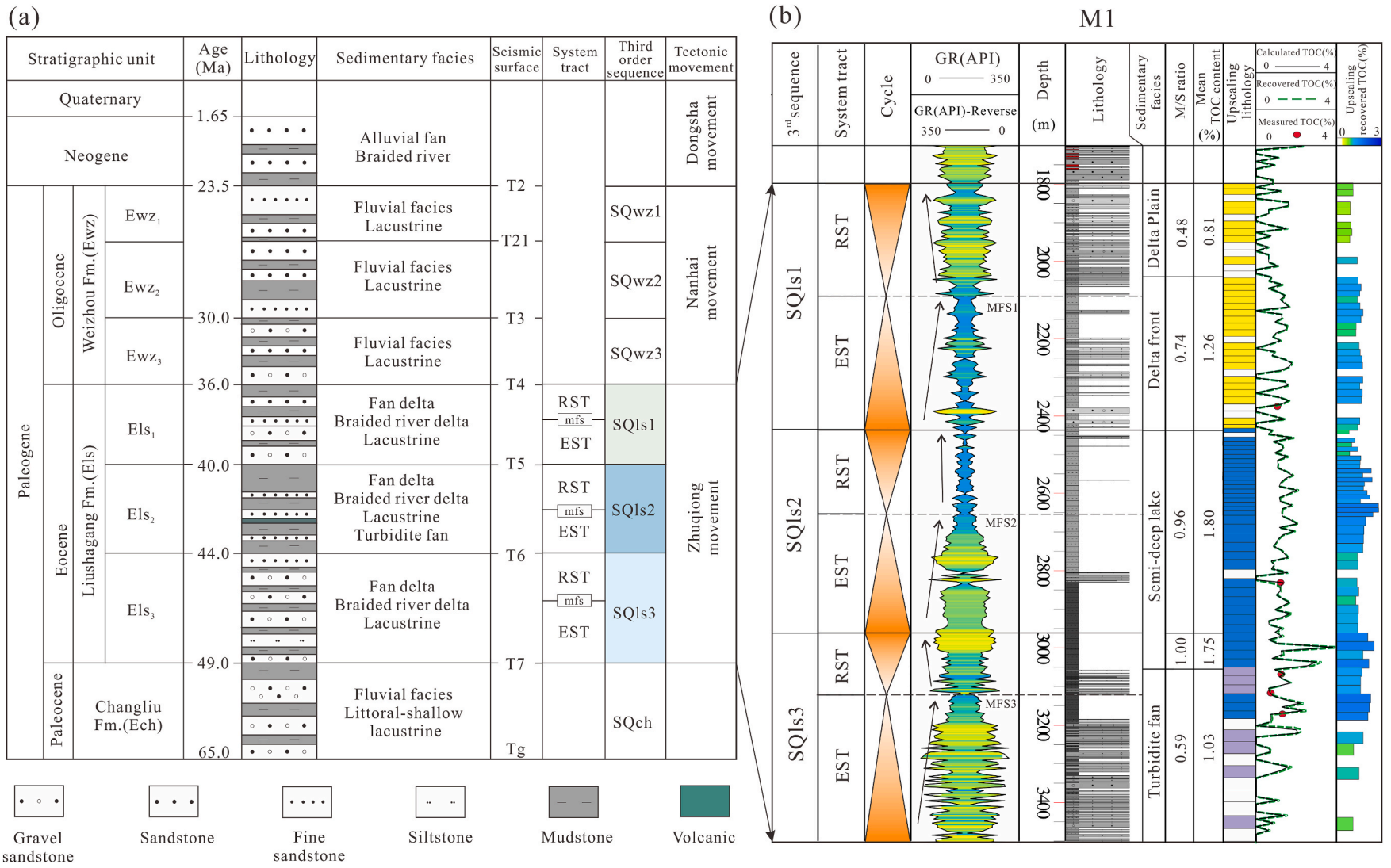

Fig. 2. (a) Generalized stratigraphic column and sequence evolution of the Fushan Depression (Zeng et al., 2022b). (b) Profiles of stratigraphic sequence division and geochemical characteristics of well M1. M/S ratio: mudstone to stratum thickness ratio.

Table 1
Element content of the selected mudstone samples.

Well	Sequence	Depth (m)	Mudstone types	H/C	O/C
C12x	SQls1-RST	2545.20	FDFM	1.11	0.11
C12x	SQls2-RST	3473.50	FDFM	1.19	0.06
C2	SQls1-RST	2491.50	FDFM	1.29	0.10
HG5	SQls3-RST	2732.00	SLM	0.95	0.09
HG5	SQls3-RST	2733.50	SLM	1.11	0.11
J2x	SQls2-RST	3562.20	FDFM	1.08	0.04
M1	SQls1-EST	2383.34	DFM	1.10	0.14
M1	SQls3-EST	3169.48	DFM	1.08	0.07
M12ax	SQls3-EST	2660.00	DFM	1.12	0.10
M17x	SQls3-EST	3799.20	SDLM	1.26	0.04
M17x	SQls3-EST	3803.50	SDLM	1.28	0.04
Y10x	SQls1-EST	3499.70	TBFM	0.95	0.04
Y10x	SQls1-EST	3539.50	TBFM	0.90	0.05
Y11x	SQls1-RST	3290.50	TBFM	0.93	0.06
Y11x	SQls1-RST	3318.20	TBFM	0.98	0.06
Y11x	SQls1-EST	3649.30	SDLM	0.88	0.04
Y11x	SQls1-EST	3654.90	SDLM	0.83	0.04
Y11x	SQls1-EST	3707.80	SDLM	0.87	0.07
Y11x	SQls1-EST	3727.00	SDLM	0.95	0.07
Y13x	SQls1-RST	3586.66	TBFM	0.99	0.07
Y7x	SQls2-RST	3784.88	TBFM	0.85	0.05

Note: FDFM= Fan delta front mudstone; SLM= Shallow lake mudstone; DFM = Braided river delta front mudstone; SDLM: Semi-deep lake mudstone; TBFM = Turbidite fan mudstone.

distribution and quantity of effective source rocks using comprehensive available data.

Combining sequence stratigraphy with geochemical analysis has been suggested by several geologists as successful method for evaluating marine source rocks (Peters et al., 2000; Makled et al., 2018; Kassem et al., 2022; Diab et al., 2023). This is due to the regularity in distribution and quality of marine source rocks within the sequence stratigraphic framework (Lai et al., 2020a, 2020b). However, evaluating lacustrine source rocks presents significant challenges due to the depositional process being heavily influenced by paleoclimate, paleoenvironment, and frequent fluctuations in lake levels. (Thiry, 1989; Aziz et al., 2003; Ribes et al., 2015). This leads to significant complexity, variability, and heterogeneity in their occurrence and geochemical properties. In addition, the multi-directionality of the provenance system resulting from complex tectonic evolution further complicates the study of effective source rocks. (Li et al., 2017; Zeng et al., 2022a). Traditionally, it is believed that lacustrine effective source rocks are mainly found in deep to semi-deep lakes and steep slope zones, while they are absent from gentle slope zones due to shallow water not being favorable to the preservation of organic matter (Qin, 2005). However, recent studies have found that effective source rocks in certain areas are pro-deltaic mudstones located in gentle slope zones, with higher hydrocarbon generation potential than previously thought (Lai et al., 2020c; Liu et al., 2022).

Accurate characterization of reservoirs' physical and fluid properties through three-dimensional modeling has the potential to enhance production efficiency and optimize resource recovery (Ali et al., 2022). Similarly, employing three-dimensional modeling to assess the distribution of source rock and its geochemical properties can facilitate precise estimations of resource volumes and predictions pertaining to

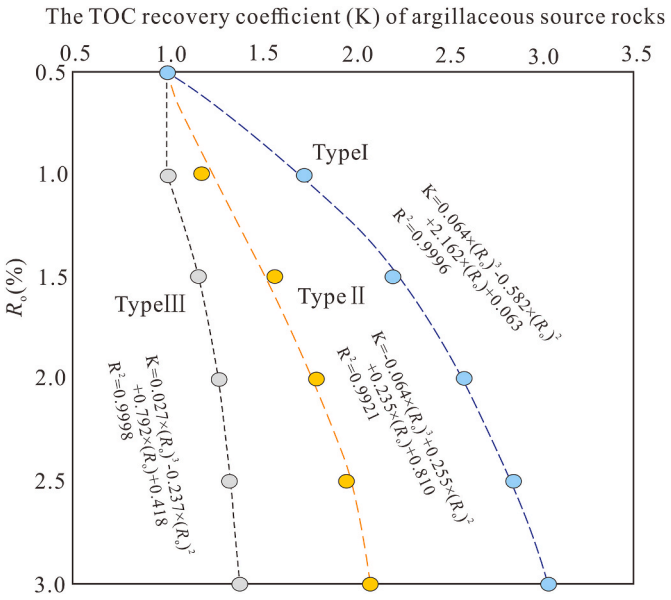

Fig. 4. TOC recovery equations for muddy source rocks of different kerogen types (Pang et al., 2014).

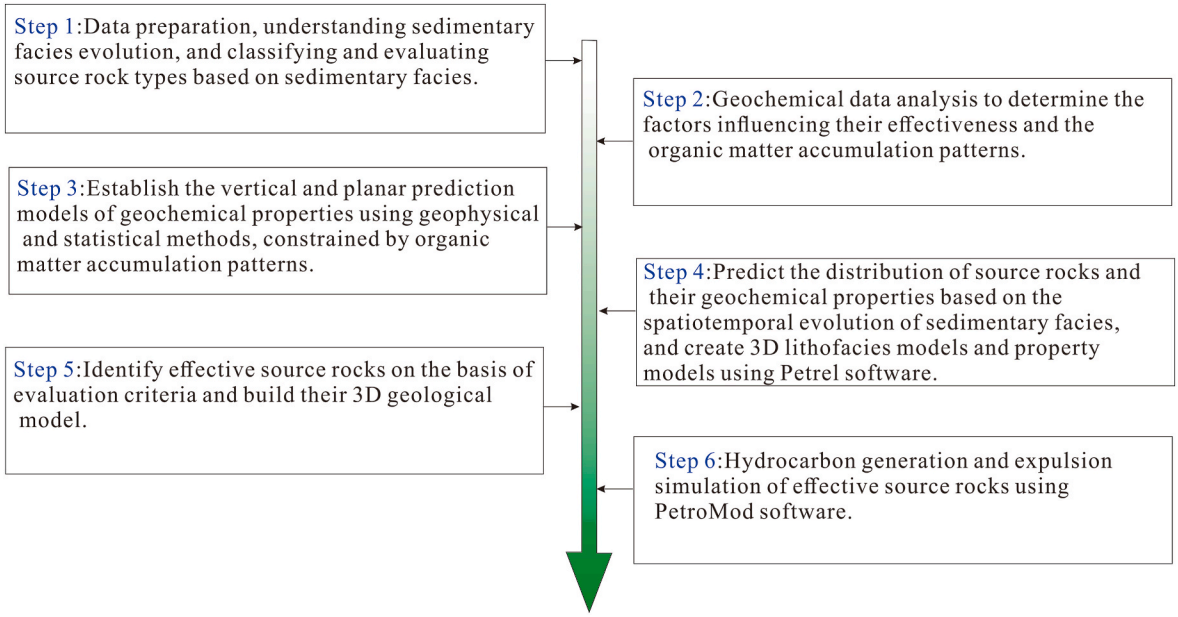

Fig. 3. Workflow for predicting effective source rocks and hydrocarbon resources potential in lacustrine basins.

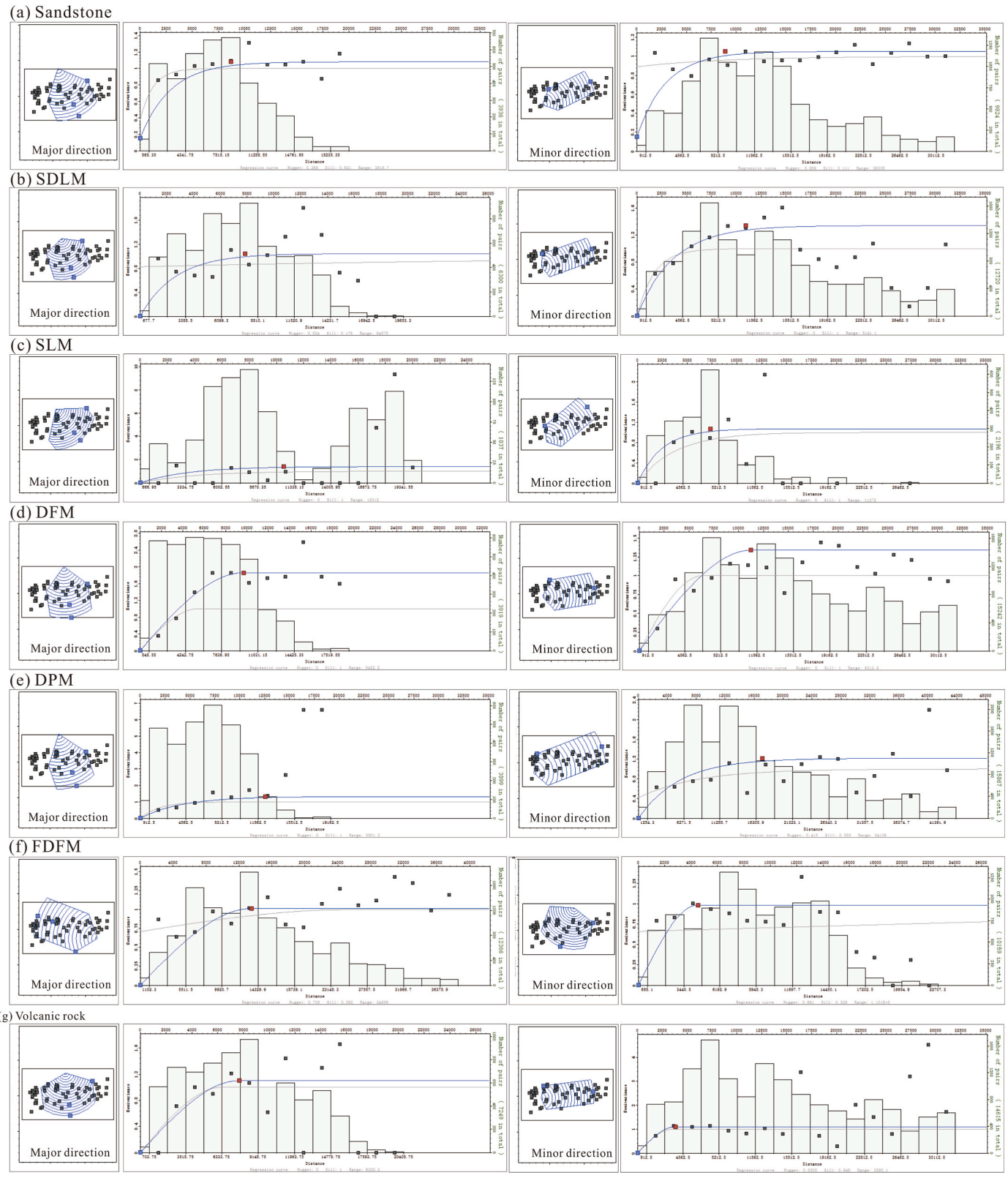

Fig. 5. Variograms of different lithofacies in the major and minor directions.

hydrocarbon accumulation distribution. Facies modeling assumes paramount significance in the characterization and comprehension of subsurface reservoirs and source rocks (Alabert and Massonnat, 1990). Presently, prominent techniques employed for simulating facies distribution encompass Sequential Indicator Simulation (SISIM), Object-based Modeling (OBM), and Multiple-Point Statistics (MPS) (Alabert and Massonnat, 1990; Seifert and Jensen, 1999; 2000; Liu et al., 2004; Al-Mudhafar, 2017). Each method possesses distinct advantages and capabilities, empowering geoscientists and petroleum engineers to effectively tackle diverse geological complexities. Rock property

Table 2
Summary of all layers modeled in the PetroMod software.

Layer name	Age at the top (Ma)	Facies assignment	PSE
Neogene and Quaternary sediments	0	Conglomerate (60%) + Sandstone (40%)	Overburden Rock
Erosion-T2	23.5	–	–
SQwz1+SQwz2	25.5	Sandstone (85%) + Shale (15%)	Overburden Rock
SQwz3	30	Sandstone (70%) + Shale (30%)	Reservoir Rock
Erosion-T4	36	–	–
SQls1-RST	37	Extracted from the Petrel project	Source Rock
SQls1-EST	38.5	Extracted from the Petrel project	Source Rock
SQls2-RST	40	Extracted from the Petrel project	Source Rock
SQls2-EST	42	Extracted from the Petrel project	Source Rock
SQls3-RST	44	Extracted from the Petrel project	Source Rock
SQls3-EST	47	Extracted from the Petrel project	Source Rock
SQch	49	Sandstone (95%) + Shale (5%)	Underburden Rock
Basement	65	Granite (150 Ma old)	Base Model

Note. -: the parameter is not set. PSE: petroleum system element.

Table 3
Summary of input parameters for intrusion modeling.

Input parameters	Units	Values
Facies	–	Volcanic
Intrusion lithotype	–	Gabbro
Age	(Ma)	31.4
Intrusion temperature	(°C)	980
Solidus temperature	(°C)	600
Magma density	(kg/m3)	2650
Magma thermal conductivity	(W/m/K)	3
Magma heat capacity	(kcal/kg/K)	0.18
Crystallization	(MJ/m3)	2

modeling endeavors to numerically simulate and model the physical attributes of rocks, such as porosity, permeability, saturation, and rock density. Sequential Gaussian Simulation (SGSIM) is a statistical-based stochastic simulation technique that accounts for the spatial variability of rock properties and the intricate nature of geological structures (Journel and Alabert, 1990; Ali et al., 2022). It is well-suited for simulating the spatial distribution of TOC.

The Fushan Depression, located in the South China Sea, is a Cenozoic lacustrine rift depression and is known for its abundant hydrocarbon resources. (Li et al., 2008). Previous studies estimated the total volume of effective source rocks in this region to be around 1775 km^3, with the second member of the Eocene Liushagang Formation being the main source layer for hydrocarbon generation (Zhang et al., 2012; Chen et al., 2015; Gan et al., 2020; Zeng et al., 2022b). However, the findings based on conventional methods are imprecise, leading to overestimation of resources and improper well placement. To address this issue, we propose a method that combines geochemical data, geophysical techniques, sedimentological theory, and statistical analysis for 3D geological modeling of effective source rocks in the Fushan Depression. By accurately identifying and quantifying effective source rocks, this method can help optimize well deployment and improve hydrocarbon resource evaluation, ultimately contributing to more efficient and sustainable exploration. This is a generally applicable method for the investigation of effective source rocks that can be used in other lacustrine basins.

2. Geological setting

The Fushan Depression is a hydrocarbon-rich rift sub-basin situated in the southern margin of the Beibuwan Basin, spanning an area of about 2920 km^2 (Fig. 1a) (Li et al., 2008; Liu et al., 2014). It is bounded by the Lingao, Ding'an, and Changliu faults to the northwest, south, and northeast, respectively. Due to multi-phase tectonic movement, the Fushan Depression has been divided into three structural units from north to south: the northern step-fault zone; the central structural zone, and the southern slope zone (Fig. 1b) (Liu et al., 2015). Separated by the Huachang transition zone, the central structural zone is further divided into two independent sags (namely the Bailian Sag in the east and the Huangtong Sag in the west). The Meitai, Hongguang, and Bailian areas in the slope zone, the Chaoyang and Jinfeng areas in the step-fault zone, and the Yong'a and Huachang areas in the central sag zone are the principal hydrocarbon-bearing regions in the Fushan Depression. (Fig. 1b).

Over 9000 m of continental sediments have been deposited in the Fushan Depression, with the sedimentary formations including the Changliu Formation in the Paleocene, the Liushagang Formation in the Eocene, the Weizhou Formation in the Oligocene, and the Neogene strata (Fig. 2a) (Li et al., 2008). This study focuses on the Liushagang Formation (500–2000 m thick) (Fig. 1c), which is the major hydrocarbon-generating bed and reservoir in the Fushan Depression (Zeng et al., 2022b). The Liushagang Formation is comprised of three members (Els3, Els2, and Els1), which correspond to three third-order sequences (SQls3, SQls2, and SQls1) (Fig. 2a) (Ma et al., 2012). Two system tracts, i.e. the expanding system tract (EST) and the regressive system tract (RST), can also be identified in each sequence depending on the variations observed in natural gamma logging and the stacking patterns that indicate retrogradation or progradation (Fig. 2b). The Liushagang Formation is made up of lacustrine sediments with deltaic deposits, as reported by Li et al. (2017). A large-scale braided river delta originating from the southern provenance was identified in the slope zone, while fan delta facies were deposited in the step-fault zone. Lacustrine facies and turbidite fans comprising dark mudstones and siltstone interbeds were mainly formed in two sags (Liao et al., 2015). The sequence division and sedimentary evolution of the Liushagang Formation are shown in Fig. 1d and e.

3. Data and methods

3.1. Data base

This study utilized geochemical data from 196 source rock samples, encompassing measurements of TOC content, S_1, S_2, HI (hydrogen index), and T_{max} (temperature at maximum pyrolysis yield) (from Zeng et al., 2022a). The vitrinite reflectance (*Ro*) data of 41 mudstone samples from various tectonic units were obtained from Zeng et al. (2022b) and Gan et al. (2020). Elemental analysis of organic matter was conducted using an elemental analyzer, with the results summarized in Table 1. Additionally, well data from 61 wells were collected, including well tops, well paths, and logging data (gamma-ray, resistivity, and sonic logs) as well as check shots. The well locations are illustrated in Fig. 1c. Seismic data from a 3D survey were utilized for geological modeling, while maps of the depositional facies and the mudstone to stratum thickness ratio (M/S ratio) isolines were obtained from the Southern Oil Exploration and Development Company, PetroChina.

3.2. Workflow

Organic matter accumulation patterns are controlled by productivity and preservation conditions within various sedimentary facies, which significantly contributes to the heterogeneous distribution of effective source rocks (Pedersen and Calvert, 1990; Sageman et al., 2003; Mort et al., 2007). To improve the accuracy of prediction results, this study

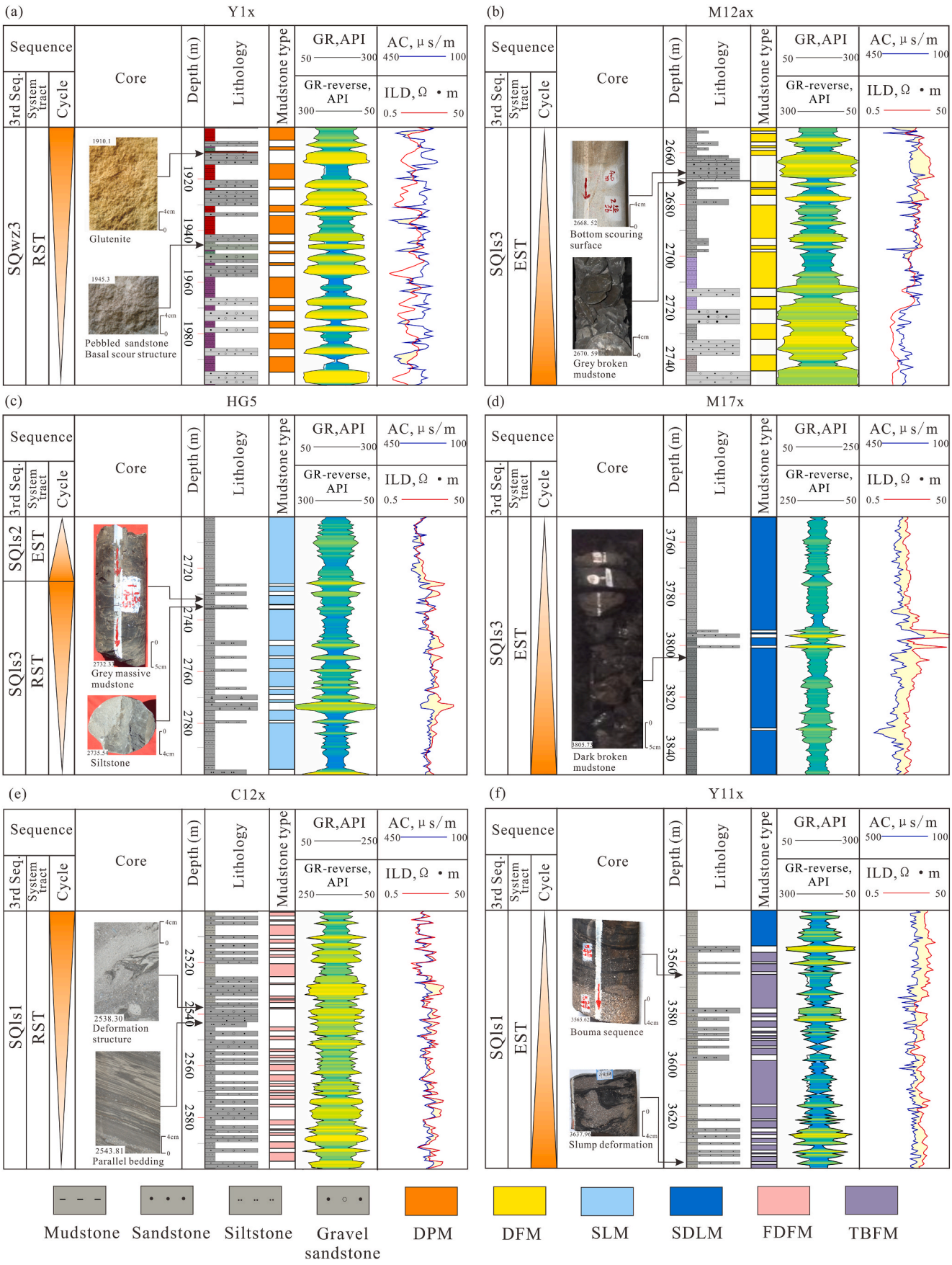

Fig. 6. Lithological and logging characteristics of various types of mudstones in representative wells.

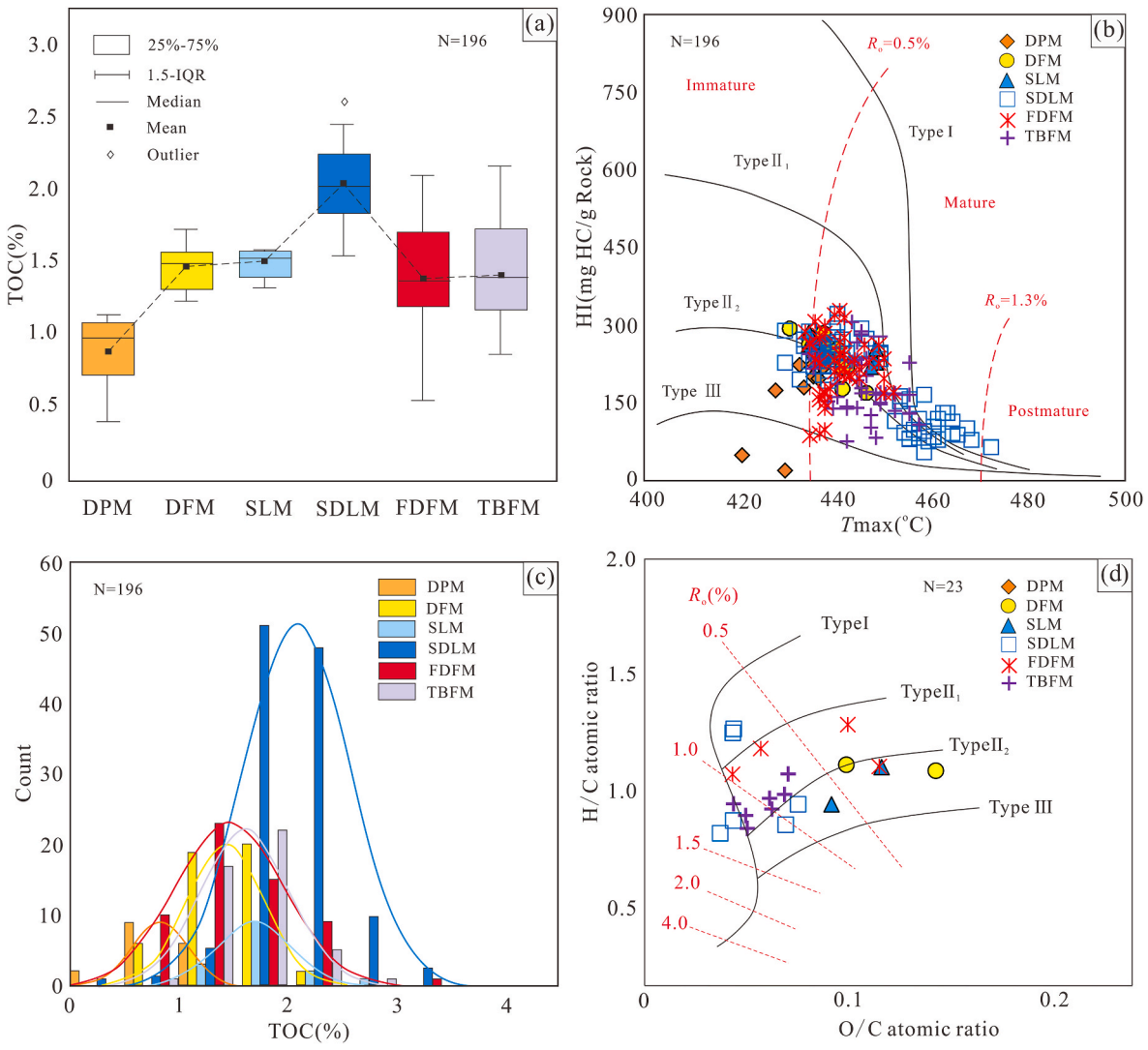

Fig. 7. (a) Box plot of mudstone types and TOC contents. (b) Cross-plot of HI versus T_{max} of mudstones (Bordenave et al., 1993). (c) Histogram showing the normal distribution of TOC contents for each type of mudstones. (d) Cross-plot of kerogen atomic H/C versus O/C (Peters, 1986).

used facies-controlled modeling to enhance the correlation between geophysical techniques and geological theory. The organic matter accumulation patterns of source rocks in various sedimentary environments are derived from Zeng et al. (2022a). The workflow for predicting effective source rocks and hydrocarbon resource potential is shown in Fig. 3.

3.3. Estimation and recovery of TOC content

In this research, we utilized a logging-based model to estimate the total organic carbon (TOC) content in the frequently alternating sandstone and mudstone formations of the Fushan Depression. Surface fitting techniques were employed to adapt the model to the lacustrine environment, enabling accurate evaluation of the vertical variations in TOC content (Zeng et al., 2021). TOC curves were computed for 61 wells and then used to estimate initial TOC contents using the TOC recovery equations proposed by Pang et al. (2014), which were based on the characteristics of hydrocarbon source rocks in numerous lacustrine basins in eastern China (Fig. 4). Vitrinite reflectance (*Ro*) curves were generated using the numerical correlation between *Ro* values and depths. Furthermore, to better understand the planar distribution of organic matter, the study utilized the numerical relationship between TOC contents and the M/S ratios for quantitative assessment (Zeng et al., 2022a). This approach helped to provide constrained trends for modeling geochemical properties.

3.4. Static 3D stratigraphic modeling

The facies-controlled modeling approach involves interpolating petrophysical parameters, such as porosity and permeability on the basis of the sedimentary facies type (Seifert and Jensen, 2000; Li et al., 2006; Zhang et al., 2008; Radwan et al., 2022; Abdullah et al., 2022; Abdelmaksoud and Radwan, 2022; Ali et al., 2022), as the expected value and variance of these parameters vary with different facies types. In this study, we sought to verify the applicability of facies-controlled modeling to geochemical parameters, specifically the TOC content, using measured data. The facies-controlled modeling process consists of three main components: structural modeling, source rock framework (lithofacies modeling), and geochemical property modeling. To perform 3D geological modeling, the following steps were taken: (1) Auditing and quality checking of logging information and seismic data. (2) Integration of seismic data interpretation, including seismic-to-well ties, horizons (top and bottom surfaces of different system tracts of the Liushagang sequences), and fault modeling, to build two-way time (TWT) surfaces, which were then converted to depth surfaces using an advanced velocity model. Structural modeling was obtained after fault modeling, pillar

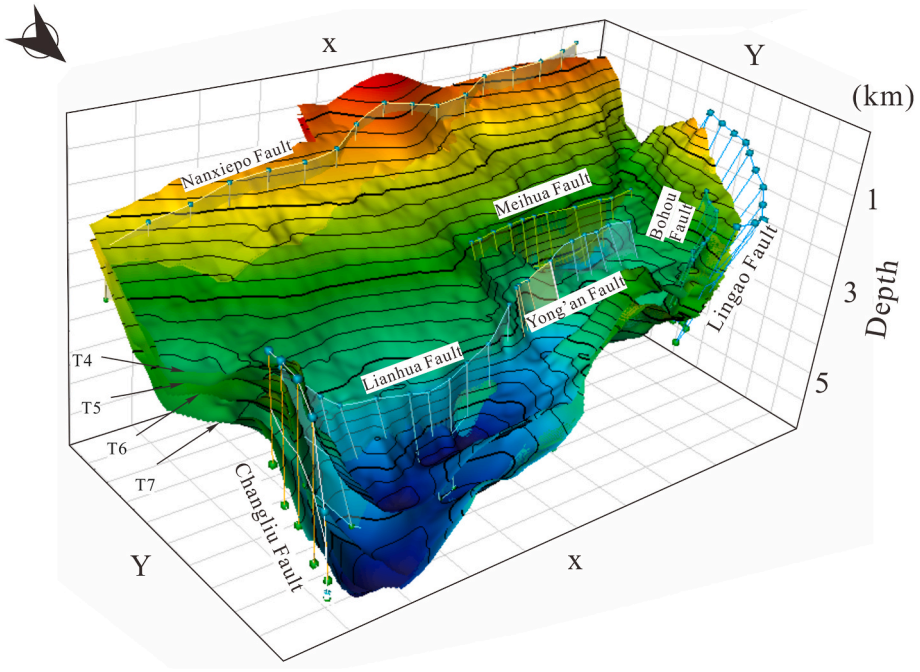

Fig. 8. 3D structural model showing horizons and major faults of the Liushagang Formation in the Fushan Depression. The scope of the model is illustrated in Fig. 1.

gridding, and formation extraction. Each system tract unit was further divided into dozens of sublayers, with 10–30 m thickness, to improve vertical accuracy, (3) Definition of sedimentary facies characteristics, lithofacies classifications (Sandstones and different types of mudstones), and upscaling based on core data, lithology logging data, and regional depositional settings (Ma et al., 2012; Liao et al., 2015; Li et al., 2017) (Fig. 2b). The identification criteria for different lithofacies can be found in Section 4.1. A 3D distribution model of lithofacies was established using Sequential Indicator Simulation (SISIM) based on data analysis, with manual adjustments made according to geological theories and sedimentary facies research achievements. In this study, the vertical lag distance was assigned as cell thickness, with the major direction being the provenance direction. The modeled indicator variograms of different lithofacies are shown in Fig. 5. Considering the validity of the model, we selected 56 wells as model wells and 5 wells located in different positions as validation wells. Based on data analysis, we performed 20 simulations using SISIM and selected the model that best matched the expected outcomes as the final result. (4) Thermal maturity and initial TOC content modeling were carried out to establish the geochemical property model. A thermal maturity model was established based on the mathematical correlation between *R*o value and depth. Furthermore, by fitting the variograms of TOC for various lithofacies, a TOC content model was developed using Sequential Gaussian Simulation (SGSIM) in alignment with the facies model. The modeling process incorporated the spatial distribution trend obtained in Section 3.3 as a constraint. The validation methods for assessing the effectiveness of the model are consistent with Step 3. All modeling steps were implemented using the Petrel software (version 2018) from Schlumberger.

3.5. Dynamic hydrocarbon generation and expulsion simulation

Basin and Petroleum System Modeling (BPSM) is a robust methodology that can be employed to examine the temporal and spatial evolution of sedimentary basins, enabling the analysis of hydrocarbon generation, expulsion, migration, accumulation, and preservation (Peters et al., 2012; Zeinalzadeh et al., 2015). In this study, simulation and calculation processes were conducted using the PetroMod software (from Schlumberger; version 2016), following the procedures described by Allen and Allen (2015) and Ruggieri et al. (2022). (1) Geological models, including structural models, fault systems, lithofacies models, and initial TOC content models, were extracted from the Petrel project. The age assignment and petroleum system elements are presented in Table 2. The erosion thickness was defined vertically by the interval transit-time approach and regionally by the interpolation method, respectively (Magara, 1976). (2) Since this study focused on hydrocarbon generation and expulsion, facies petrophysical properties such as porosity and permeability were assigned using empirical values from the software. (3) Source rock parameters, including hydrogen index (HI) and organic matter type were assigned based on experimental data (Zeng et al., 2022a), using a HI of 300 mg HC/g TOC, a type II kerogen, and a kinetic model from the PetroMod catalog (Burnham, 1989 *T*-II), which corresponds to general type II kerogens. Organic maturity was calculated overlying EASY %*R*o model of Sweeney and Burnham (1990). (4) The main boundary conditions of BPSM, such as paleo water depth (PWD), sediment water interface temperature (SWIT), and heat flow (HF), were determined. The PWDs for each system tract unit were assigned based on the different depositional environments (Chen et al., 2002). The SWITs were calculated according to the global mean temperature at sea level reported by Wygrala (1989) for the latitude of 20° in Eastern Asia. Six wells from different tectonic units were selected as representative locations for 1-D BPSM to reconstruct the burial and thermal history and obtain Paleo-heat flows, corrected by *R*o values (Tawfik et al., 2022; Hakimi et al., 2022). Planar heat flow maps at critical geological times were drawn using the interpolation method. (5) The faults were set to "open" only during the hydrocarbon charging period (Wang et al., 2022). (6) The emplacement of igneous intrusions within host rocks is commonly regarded as an instantaneous process (Bruce and Huppert, 1990). The intrusion model parameters were assigned according to the values shown in Table 3 (Friedmann et al., 1981; Monreal et al., 2009; Liu et al., 2017).

4. Results

4.1. Classification of mudstone types

For the study area, we identify six distinct types of probable source rocks (mudstones) within the Liushagang Formation based on their sedimentary characteristics. The lithological and logging characteristics

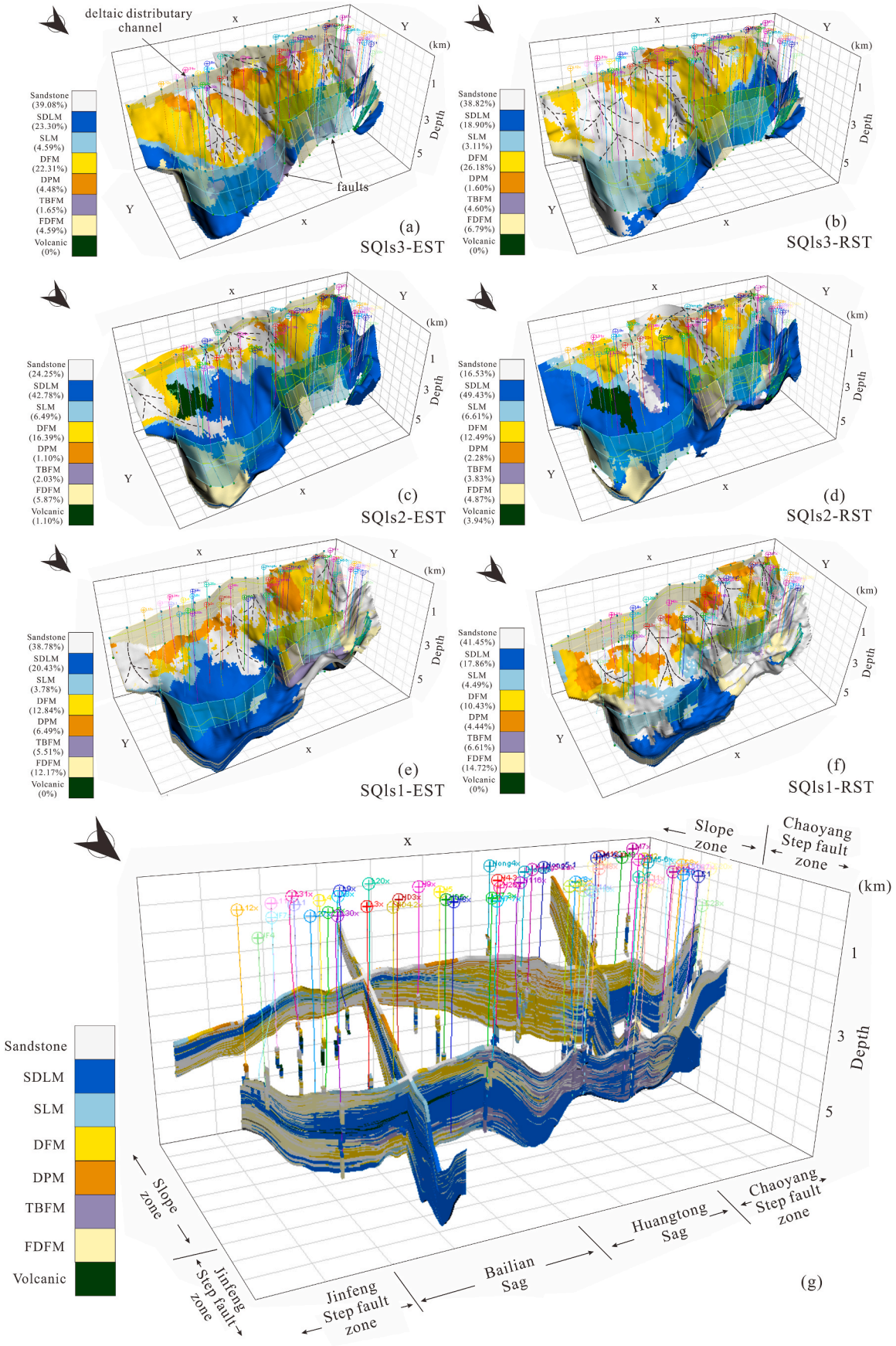

Fig. 9. (a)–(f) Facies models of different system tracts of three Liushagang sequences. (g) Fence diagram of the facies model. The scope of the model is illustrated in Fig. 1.

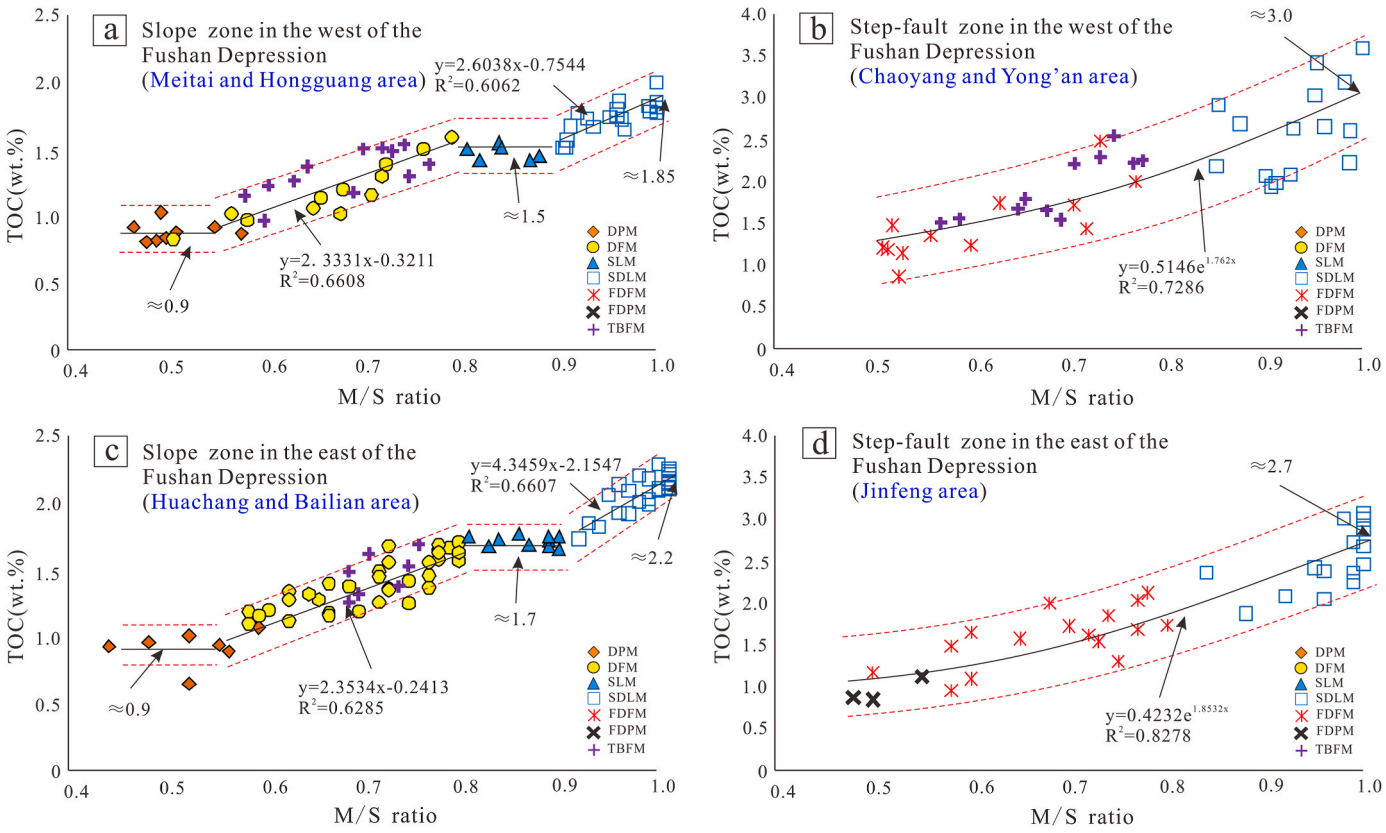

Fig. 10. Numerical relationships of different tectonic units between TOC content and M/S ratio.

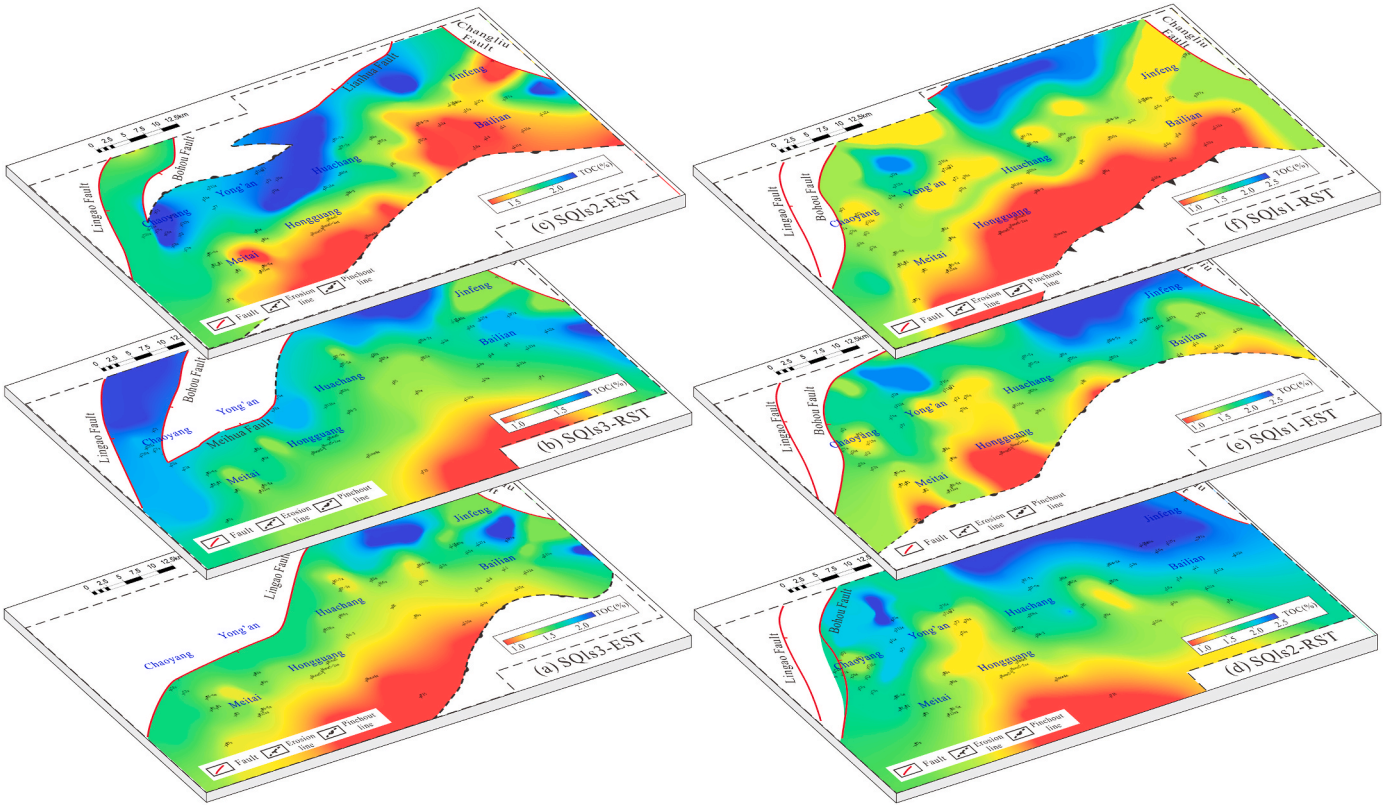

Fig. 11. Maps showing the planar distribution of TOC content of the Liushagang sequences.

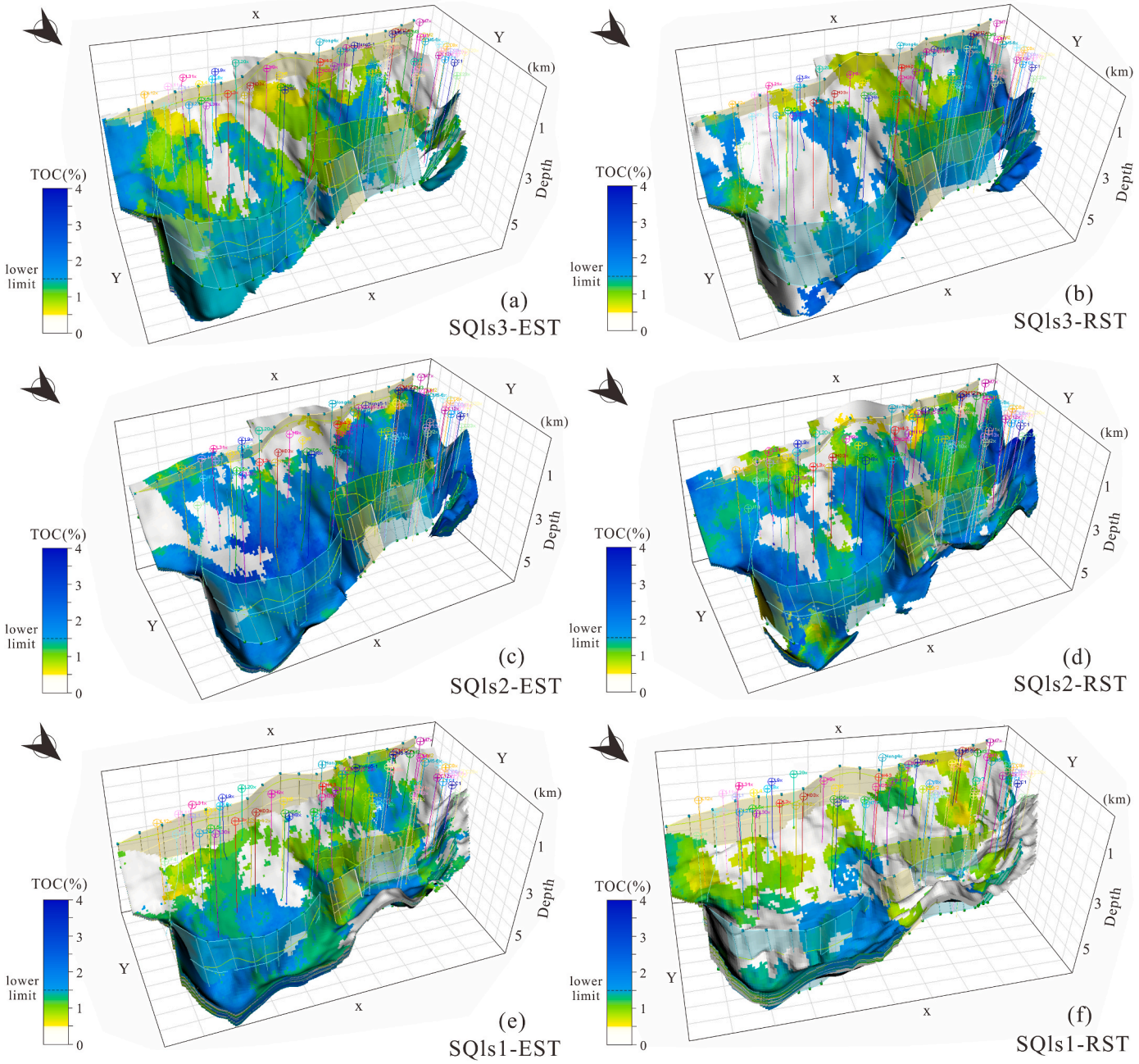

Fig. 12. TOC content models showing the spatial variation of TOC values in the Liushagang sequences. The scope of the model is illustrated in Fig. 1.

of each source rock are described in detail below. (1) Deltaic plain mudstones (DPM) were deposited in braided river delta plain environments and are locally distributed in the southern part of the study area. These mudstones are characterized by thin maroon- or light green-colored interbeds in major deltaic sandstones, which can be identified by the medium amplitude box-shaped natural gamma ray (GR) logging curves and the basal scour structures of the cores (Fig. 6a). (2) Deltaic front mudstones (DFM) originated in braided river delta front environments and are widely distributed in the slope zone. They are light grey and have bell- or funnel-shaped GR curves (Fig. 6b). (3) Shallow lake mudstones (SLM) were deposited in lacustrine shallow-water environments and consist of grey-colored muddy or silty deposits interspersed with fine-grained sandstones. Their GR curves generally show a finger shape (Fig. 6c). (4) Semi-deep lake mudstones (SDLM) were formed in lacustrine deep-water environments and consist mainly of thick dark mudstones with occasional siltstone interbedding. The GR curve is linear with low amplitude (Fig. 6d). (5) Fan delta front mudstones (FDFM) were formed in the step-fault zone with a fan deltaic depositional paleoenvironment. They are repeatedly stacked with sandstones and conglomerates in the vertical direction and have medium-to low-amplitude serrated bell- or box-shaped GR curves (Fig. 6e). (6) Turbidite fan mudstones (TBFM) were formed in the central part of the depression with a relatively deep-water environment. They are characterized by dark massive mudstones with sandstone intervals and thin, finger-shaped GR curves. Primary identification indicators of cores are the Bouma sequence and the slump deformation structure (Fig. 6f).

4.2. Geochemical characteristics of various mudstones

TOC content is a common index to assess the organic matter richness of source rocks (Tissot and Welte, 1984). However, since the TOC content in source rocks can be reduced due to hydrocarbon generation, it is

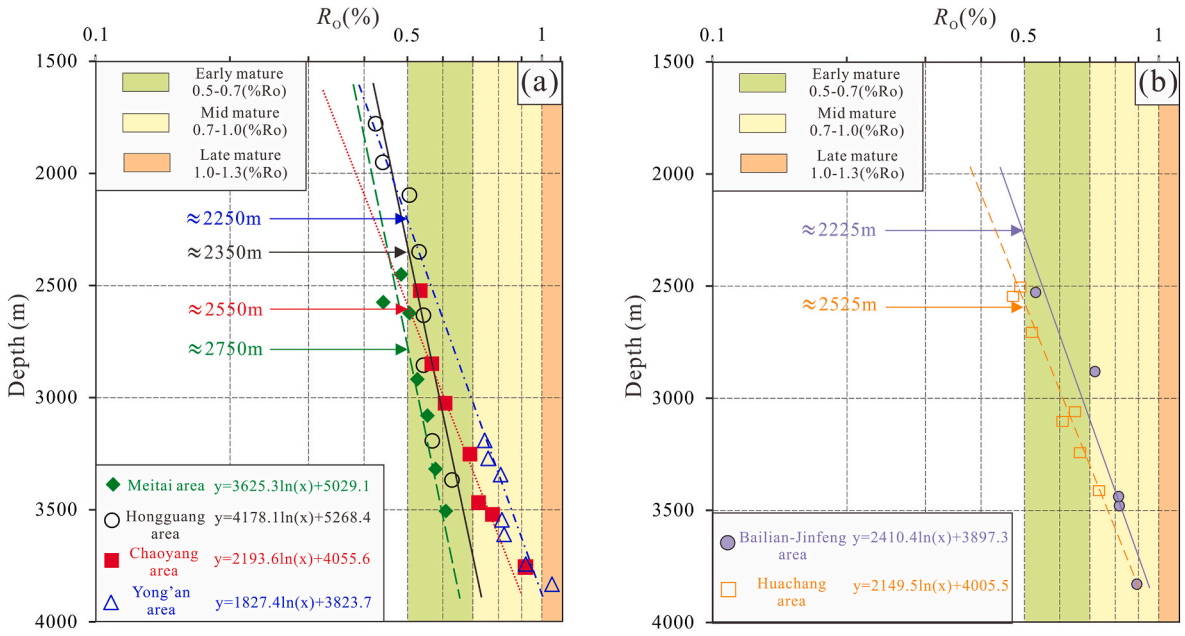

Fig. 13. Fitting between *Ro* values and corresponding depths of representative wells in different structural units.

necessary to convert current TOC values to initial TOC values before evaluation and modeling. In this study, a box plot describing the dispersion of a set of data was used to evaluate the distribution and stability of TOC content (Fig. 7a). The TOC values for the six types of mudstone samples in the study area range from 0.35% to 2.51%, with an average of 1.51%. SDLMs exhibit the highest abundance of organic matter, with TOC values ranging from 1.32% to 2.51%, an average of 1.80%, and a median of 1.78%. The SLMs have a limited range of TOC values (1.3%–1.55, average 1.48%, median 1.51%) owing to steadily improving preservation conditions and a corresponding reduction of terrigenous organic matter (Zeng et al., 2022a). DFMs, FDFMs, and TBFMs have moderate organic matter richness, with TOC contents varying widely from 1.28% to 1.70%, 0.52%–2.07%, and 0.82%–2.13%, respectively, with averages of 1.48%, 1.36%, and 1.39%. Organic matter is observed to be less abundant in DPMs, with TOC values predominantly <1%, indicating a poor hydrocarbon generation potential. In summary, the TOC content distribution of each type of mudstones conforms to the normal distribution, proving the feasibility of facies-controlled modeling for TOC contents (Fig. 7c).

The kerogen type is another geochemical parameter that affects the effectiveness of hydrocarbon source rocks (Tissot and Welte, 1984; Hunt, 1979). In general, source rocks are distinguished as oil-prone, mixed and gas-prone types, corresponding to type I, type II and type III kerogens, respectively. In this study, the Rock-Eval pyrolysis parameters (HI and T_{max}) and organic element compositions were used to classify kerogen types in this study (Bordenave et al., 1993; Peters, 1986). The cross-plots of HI versus T_{max} and atomic H/C versus O/C indicate that all types of mudstones are dominated by type II kerogens with moderate HI values (Fig. 7b and d). As a result, it is concluded that the source rocks of the Liushagang Formation have comparable hydrocarbon generation kinetic characteristics, and the organic matter type does not significantly affect the effectiveness of source rocks in comparison to TOC content and maturity. Thus, a unified kinetic model for various mudstone types was defined for hydrocarbon generation simulation.

4.3. 3D geological modeling

4.3.1. Structural model

A realistic high-resolution 3D structural model of the stratigraphy is essential for accurately locating source rocks and reservoirs (Khattab et al., 2023). Seven major faults, namely Lingao Fault, Changliu Fault, Meihua Fault, Lianhua Fault, Yong'an Fault, Bohou Fault, and Nanxiepo Fault, were defined in the structural model by synthesizing and editing "Key Pillars" as illustrated in Fig. 8. These faults are mainly oriented perpendicular to the major provenance direction (W-E and SW-NE) and have a significant influence on the deposition of the study area. The stratigraphic horizons were loaded into a 3D grid, each one with a cell size measuring 200 m × 200 m. Using this model, the volumes of SQls3-EST, SQls3-RST, SQls2-EST, SQls2-RST, SQls1-EST, and SQls1-RST were calculated as 311.45 km^3, 327.50 km^3, 209.74 km^3, 257.20 km^3, 245.96 km^3, and 238.78 km^3, respectively.

4.3.2. Facies model

A 3D lithofacies model comprising sandstones, DPMs, DFMs, SLMs, SDLMs, FDFMs, TBFMs, and volcanic rocks was constructed to distinguish between probable source rocks and reservoir rocks and facilitate further geochemical property modeling. Sandstones were found to be abundant in SQls3-EST, SQls3-RST, SQls1-EST, and SQls1-RST, accounting for 39.08%, 38.82%, 38.78% and 41.45% of the volumes, respectively, corresponding to the periods of relatively medium to low lake level (Li et al., 2014). Note that the distribution of sandstones clearly reflects the morphology of deltaic distributary channel (Fig. 9a–f). DPMs were predominantly deposited in low-lying areas between major channels, with volume percentages always less than 6.5% within different system tract units (Fig. 9a–f). The content of DPMs is constrained by the scale of the braided river delta, resulting in a significantly greater volume proportion in SQls3 (22.31%–26.18%) compared to SQls2 (12.49%–16.39%) and SQls1 (10.43%–12.84%) (Fig. 9a–f). SLMs, FDFMs and TBFMs occurred in slope fracture belts, step-fault zones and central sags, respectively, with volume percentages ranging from 3.11% to 6.61%, 4.59%–14.72%, and 1.65%–6.61% (Fig. 9a–f). SDLMs were prevailingly deposited in SQls2 due to the expanding lake, with volume percentages higher than 40%, while they were only distributed in the central sags in SQls1 and SQls3, with volume percentages ranging from 17.86% to 23.30% (Fig. 9a–f). Furthermore, the vertical lithofacies distribution is presented in the fence diagram in Fig. 9g.

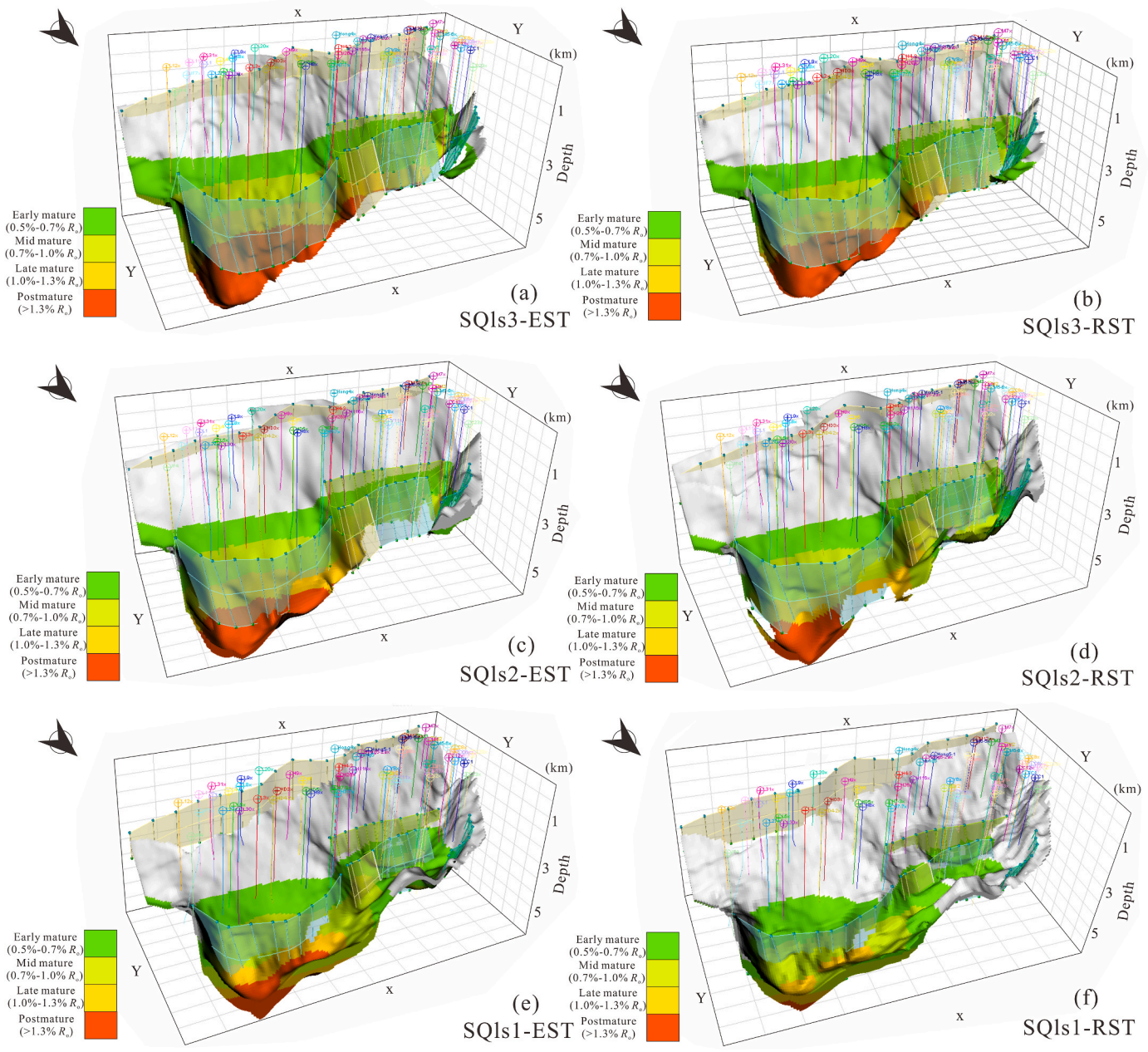

Fig. 14. Maturity models showing the thermal evolution of hydrocarbon source rocks in the Liushagang sequences. The scope of the model is illustrated in Fig. 1.

4.3.3. Geochemical properties model

Geochemical properties modeling involved assigning TOC values and maturity information to the source rock framework constructed in the lithofacies modeling. To produce a more reliable model of TOC content, the sequential indicator simulation was constrained by the trend of the TOC planar distribution. The M/S ratios and mean TOC contents of different sequences and mudstone types were calculated to quantitatively evaluate the areal distribution of organic matter (Fig. 2b). Mathematical formulas were established between the TOC content and M/S ratio for different tectonic units, which indicated that the TOC content of mudstones increased in a stepped way with the increasing M/S ratio in the slope zone, whereas it increased exponentially in the step-fault zone, consistent with the organic matter accumulation pattern of the Liushagang Formation (Fig. 10) (Zeng et al., 2022a). Contour maps of the areal TOC content, determined by the plane of M/S ratios and the prediction formulas, were generated, indicating higher TOC content values in the central and northern regions compared to the southern part (Fig. 11). 3D TOC content models of different system tracts were also presented, demonstrating an increasing trend of the TOC content toward the lake center, with greater organic matter primarily localized in the northern regions of the Fushan Depression in SQls3-RST, SQls2-EST, and SQls2-RST (Fig. 12).

Six mathematical formulas were utilized to establish a relationship between the *Ro* values and corresponding depths for six distinct tectonic units to assess the thermal maturity of the source rocks (Fig. 13). The depths at which hydrocarbon generation commences were estimated for the Meitai, Hongguang, Chaoyang, Yong'an, Bailian-Jinfeng, and Huachang regions as 2750 m, 2350 m, 2550 m, 2250 m, 2225 m, and 2525 m, respectively. Subsequently, the maturity models were established using these formulas along with the computational tool in Petrel software (Fig. 14). The study concludes that the source rocks in the Huangtong Sag and the Bailian Sag have attained the mid-mature (0.7%–1.0% *Ro*) and late-mature (>1.3% *Ro*) stage, respectively, while the occurrence of mature source rocks is scarce in the southern

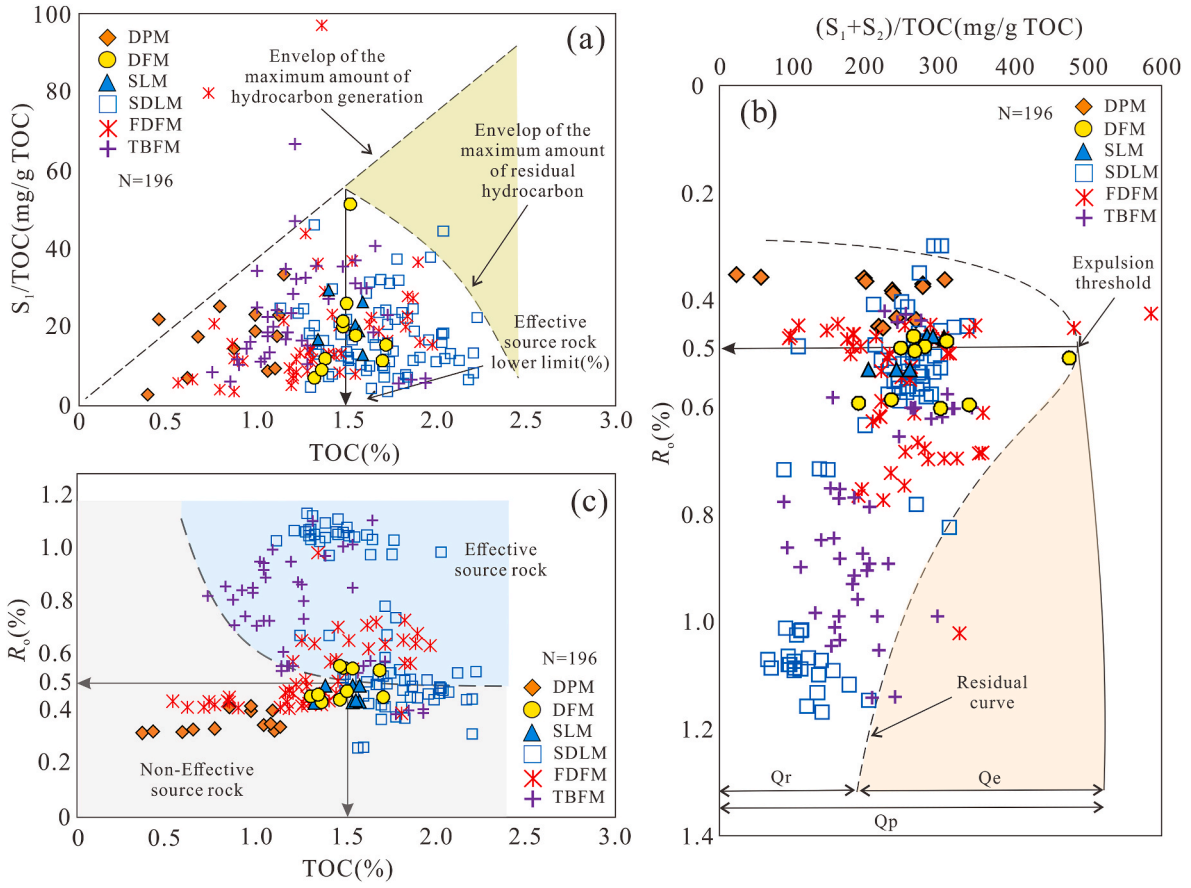

Fig. 15. (a) Schematic diagram for identifying the lower limit of TOC in effective source rocks (after Zhu et al., 2021). (b) Hydrocarbon generation potential index profile in the Fushan Depression (after Pang et al., 2005). (c) Diagrammatic identification of the effective source rocks of the Liushagang Formation (after Huo et al., 2012). Qp: amount of hydrocarbon generated. Qe: amount of hydrocarbon expelled. Qr: amount of residual hydrocarbon in the source rock.

slope zone.

5. Discussion

5.1. Identification and distribution of effective source rocks

5.1.1. Identification criteria

Effective source rocks are generally recognized according to the hydrocarbon generation and expulsion capacity of source rocks in each region (Pang et al., 2005; Zhu et al., 2021). Since this study aims to macroscopically distinguish effective and ineffective source rocks rather than obtaining accurate hydrocarbon generation and expulsion parameters, statistically based plots are used to determine the lower limit of organic carbon abundance and the threshold of hydrocarbon expulsion. In addition, hydrocarbon source rocks with different organic matter types are not discussed separately, as type II kerogens significantly dominate the mudstones of the Liushagang Formation (Fig. 7b and d).

The pyrolysis parameter S_1 represents the content of residual hydrocarbons within the source rock, indicating the amount of hydrocarbon generation when there is no expulsion. The hydrocarbon index (S_1/TOC) denotes the amount of residual hydrocarbons per unit of organic matter. In conditions involving similar types of organics, the amount of hydrocarbon generation generally increases with TOC. When the TOC is greater than the lower limit, hydrocarbons in the source rocks are expelled after filling the pores, resulting in a deviation from the original envelope line of maximum hydrocarbon production (Zhu et al., 2021). The lower limit of TOC content in the effective source rocks is determined to be 1.5% according to the schematic diagram (Fig. 15a).

The hydrocarbon generation potential index (P_g= (S_1+S_2)/TOC) refers to the quantity of volatile and pyrolytic hydrocarbons produced per unit of organic matter. Since the hydrocarbon generation process follows the principle of material balance, whereby the mass of organic matter in source rocks remains constant before and after hydrocarbon generation and expulsion (Pang, 1995). The expulsion threshold of hydrocarbons corresponds to the inflection point where the envelope curve of P_g begins to decline in the P_g and *Ro* relational graph (Pang et al., 2005). As a result, 0.5% *Ro* is defined as the expulsion threshold for identifying effective source rocks (Fig. 15b). For source rocks that meet the hydrocarbon expulsion threshold and the lower limit of organic matter abundance, TOC values decrease with increasing maturity (Fig. 15c) (Huo et al., 2012). In addition, when igneous rocks intrude into the early diagenetic stage of source rocks, they can heat and promote hydrocarbon generation in surrounding rocks up to 1–2 times the thickness of the intrusion (Simoneit et al., 1978; Othman et al., 2001). This study also identifies organic-rich mudstones (TOC>1.5%) adjacent to intrusive rocks with a thickness 1.5 times greater than the intrusion as effective source rocks.

5.1.2. Spatial distribution of effective source rocks

By integration structural models, lithofacies models, geochemical attribute models, and identification criteria, the effective source rocks are filtered and finely delineated in the Petrel software (Fig. 15). These rocks are further categorized into effective oil source rocks (TOC>1.5%, 0.5 < *Ro*<1.3%, type II kerogen) and effective gas source rocks (TOC>1.5%, *Ro*>1.3%, type II kerogen) based on their maturity, which allows for the identification of the favorable exploration areas for oil and gas, respectively (Tissot and Welte, 1984). The volume of effective source rocks is calculated by counting the number of grids, while

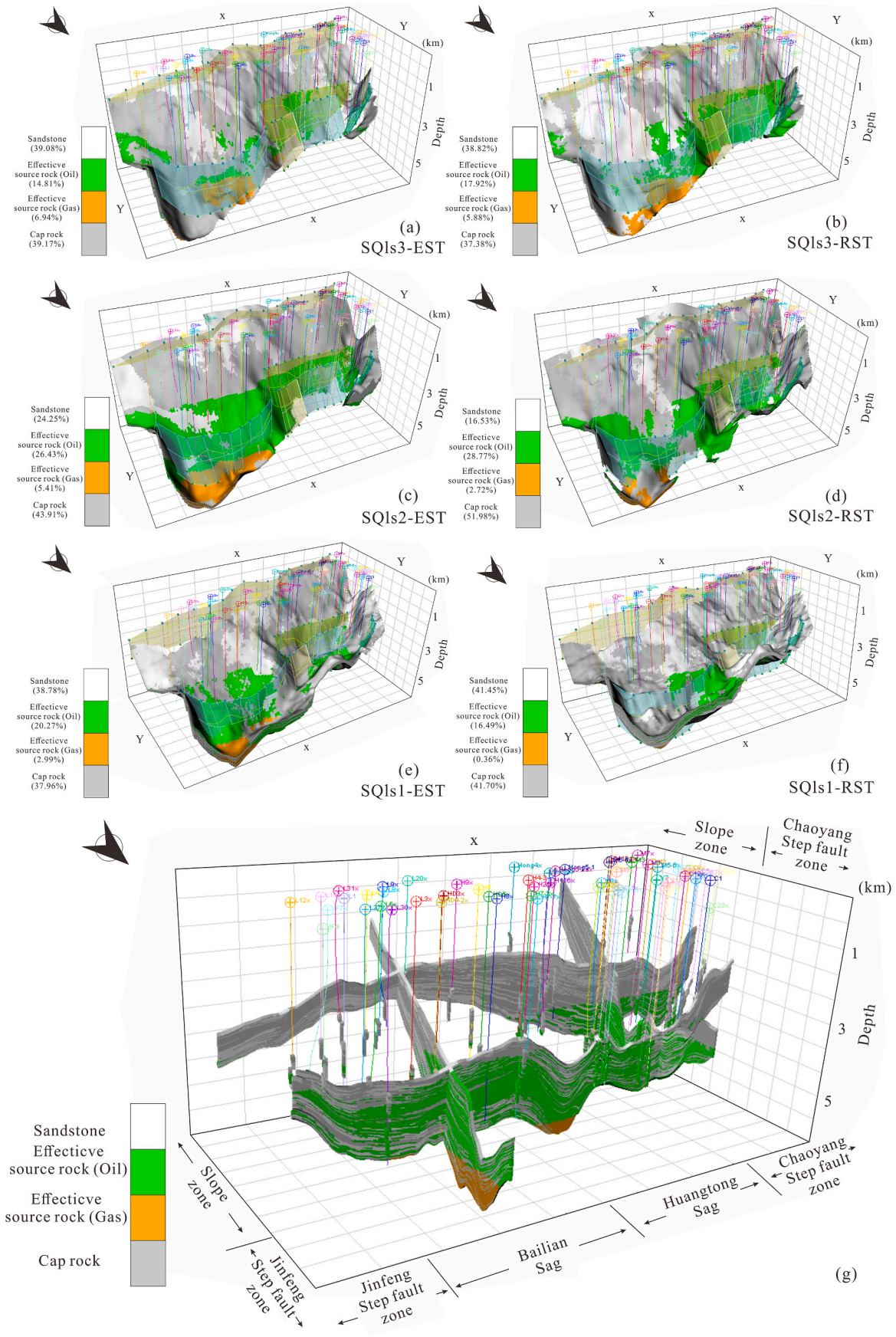

Fig. 16. (a)–(f) Effective source rock models of different system tracts of three Liushagang sequences. (g) Fence diagram of the effective source rock model. The scope of the model is illustrated in Fig. 1.

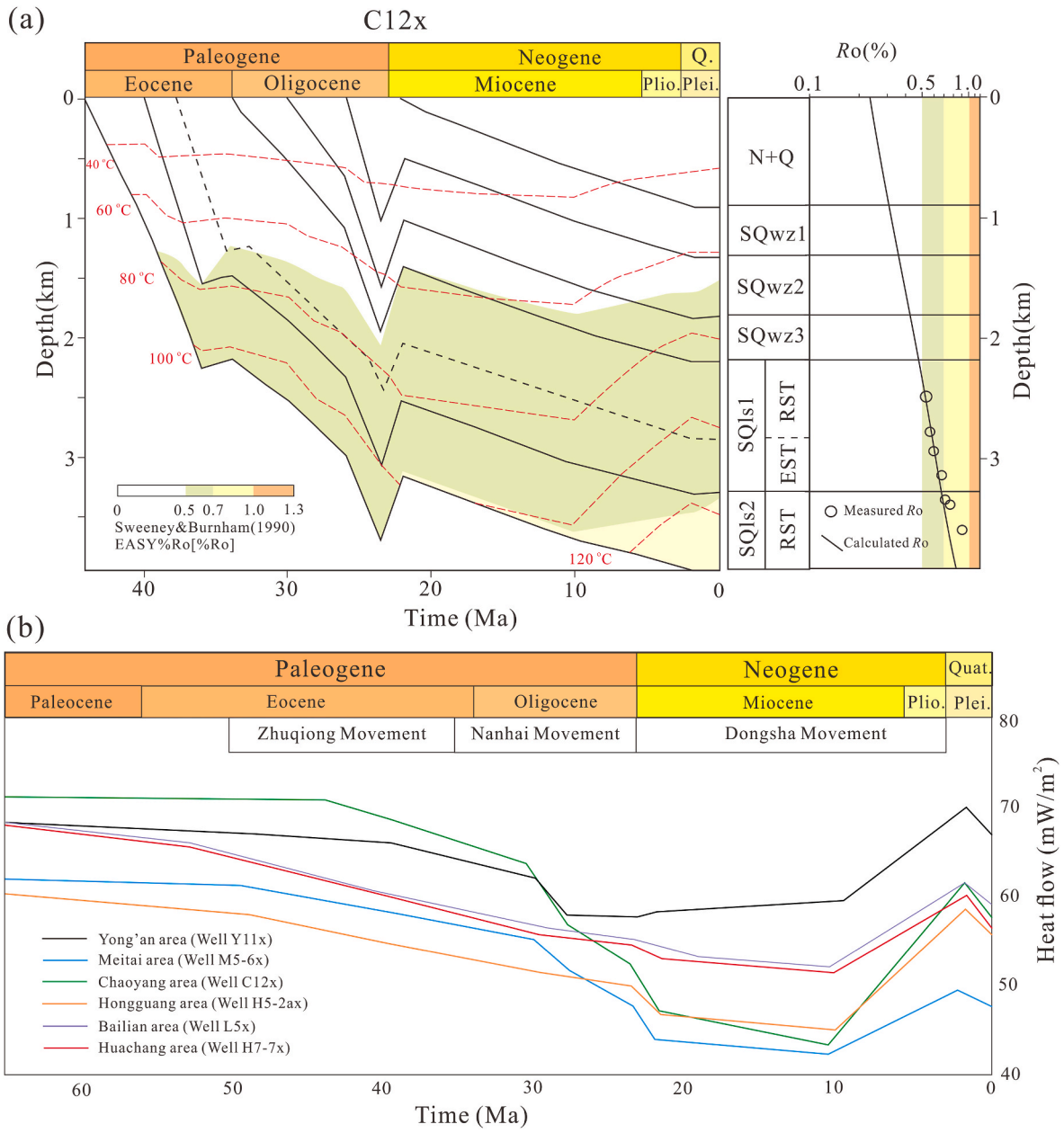

Fig. 17. (1) Burial and thermal histories of the well C12x. (2) Paleo-heat flows of six representative wells obtained by 1D-BPSM.

low-permeability rocks such as mudstones and volcanic rocks are considered cap rocks.

The southern slope zone is found to lack effective oil source rocks due to their shallow burial depth. However, effective oil source rocks are present in approximately 8–10 km wide strips to the south of the Meihua and Lianhua Faults in SQ3-EST, SQ3-RST, and SQ2-EST, with volumes of 46.13 km^3, 58.69 km^3, and 55.43 km^3, respectively (Fig. 16a–c). During the depositional period of SQ2-RST, the Hainan Uplift caused tension in the Fushan Depression while the Huangtong Sag and the Bailian Sag were formed in the north of the Meihua Fault and the Lianhua Fault, causing the lacustrine depositional center to migrate northward. A large amount of organic matter was preserved in the center of these two sags, where it was transformed into effective source rocks through geological thermal evolution. Consequently, effective oil source rocks of SQls2-RST, SQls1-EST, and SQls1-RST mainly occurred in the northern part of the Fushan Depression, with volumes of 74.00 km^3, 49.86 km^3, and 39.37 km^3, respectively (Fig. 16d and e). Effective gas source rocks, on the other hand, are limited to a small area of the northeast part of the Bailian Sag, with a total volume of 67.43 km^3 (Fig. 16), indicating that the Fushan Depression is primarily an oil-bearing basin owing to its moderate thermal evolution. The effective source rock volume derived from this study (390.91 km^3) is considerably smaller than that estimated by Zhang et al. (2012) using conventional methods (1775 km^3). The conclusion of this study is considered more accurate and scientifically rigorous than that of the previous study. The vertical distribution of effective source rocks is shown in the fence diagram (Fig. 16g), which allows for direct observation of the spatial distribution of the primary petroleum system elements, including source rocks, reservoirs, and cap layers.

5.2. *Hydrocarbon generation and expulsion potential of effective source rocks*

Reconstructing the burial and thermal histories of source rocks is a crucial step in understanding hydrocarbon generation history. As depicted in Fig. 17a, two major erosion events of the Fushan Depression

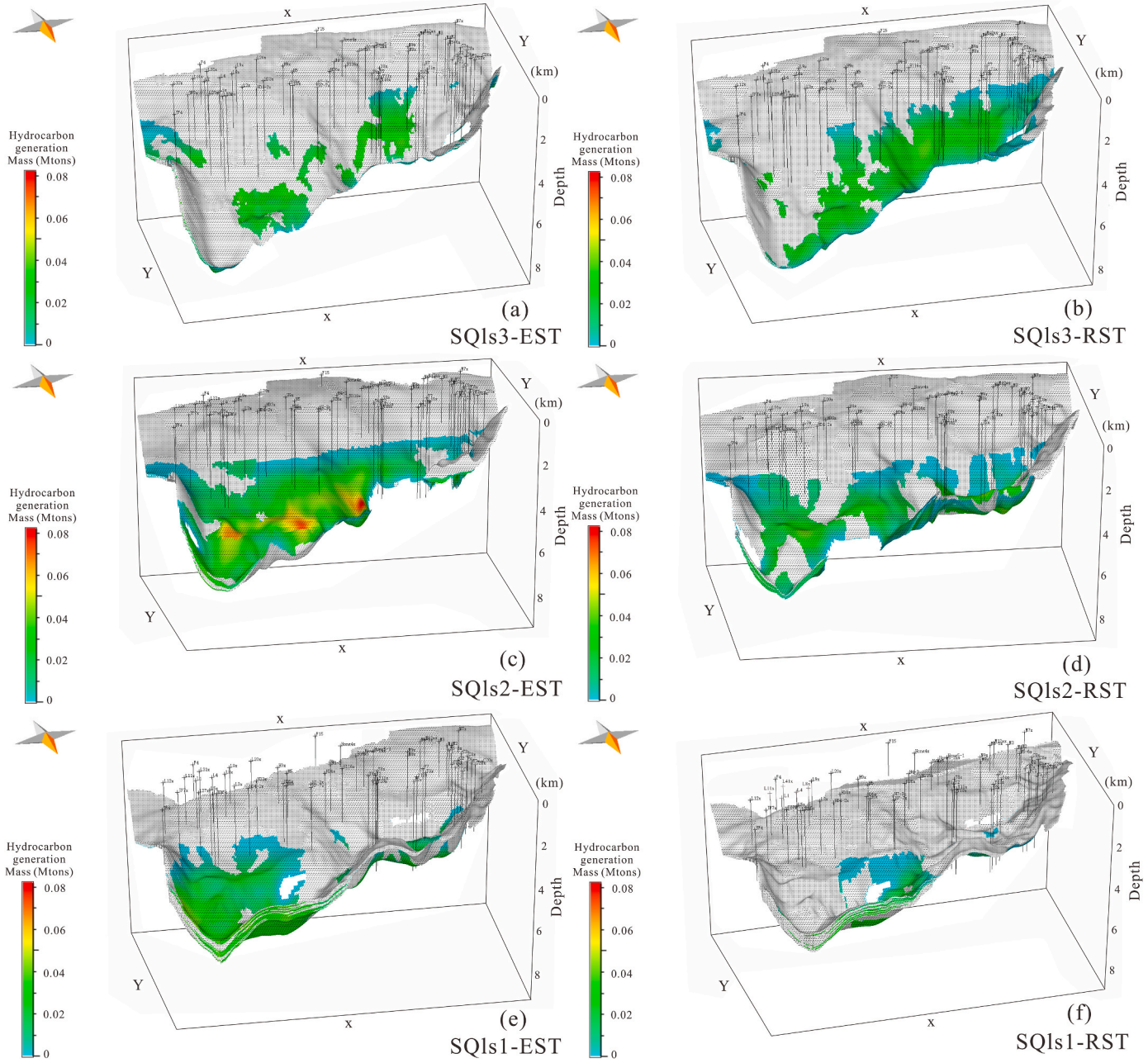

Fig. 18. 3D results of the basin simulations for the hydrocarbon generation mass of different system tract units. The scope of the model is illustrated in Fig. 1.

occurred at the end of the Eocene and the Oligocene, respectively, coinciding with the Zhuqiong Movement and the Nanhai Movement. Heat flows across different tectonic units range from 40 to 70 mW/m^2. They remained high until 30 Ma, gradually decreased during the Oligocene and the Miocene, and increased again after 10 Ma (Fig. 17b).

Three-dimensional geological models depicting the hydrocarbon generation mass within the sequence stratigraphic framework are provided in Fig. 18, indicating that SQls2-EST, SQls2-RST, and SQls1-EST are the primary hydrocarbon generating layers with large effective source rock kitchens. Fig. 19 records the amount of hydrocarbons produced by different sequences over geological time. The source rocks of the Liushagang Formation exhibit two distinct hydrocarbon generation stages of 40–25 Ma and 10–0 Ma, respectively (Fig. 19). Due to reduced heat flow and tectonic uplift, hydrocarbon generation nearly ceased during the 25–10 Ma (Fig. 17). Nevertheless, the hydrocarbon accumulations found in the Paleogene sandstone reservoirs of the Fushan Depression formed at a late stage (8–2 Ma) (Wang et al., 2022), indicating that a significant amount of early-generated hydrocarbons were either not preserved or have not yet been discovered. According to the basin simulation results, the effective source rocks of SQ3-EST, SQ3-RST, SQ2-EST, SQls2-RST, SQls1-EST, and SQls1-RST generated 852.45 megatons, 951.36 megatons, 1478.19 megatons, 1820.32 megatons, 1748.25 megatons, and 611.35 megatons of oil, respectively, with corresponding expulsion mass of 846.04 megatons, 943.16 megatons, 1464.97 megatons, 1799.9 megatons, 1727.81 megatons, and 597.23 megatons (Fig. 19a). In contrast, natural gas is relatively scarce in the Fushan Depression, with 190.27 billion m^3, 213.34 billion m^3, 337.91 billion m^3, 515.48 billion m^3, 398.16 billion m^3, and 134.98 billion m^3 produced by the system tract units from bottom to top, respectively (Fig. 19b). The corresponding natural gas expulsion volumes are 187.17 billion m^3, 209.57 billion m^3, 331.97 billion m^3, 508.24 billion m^3, 391.88 billion m^3, and 131.12 billion m^3. Therefore,

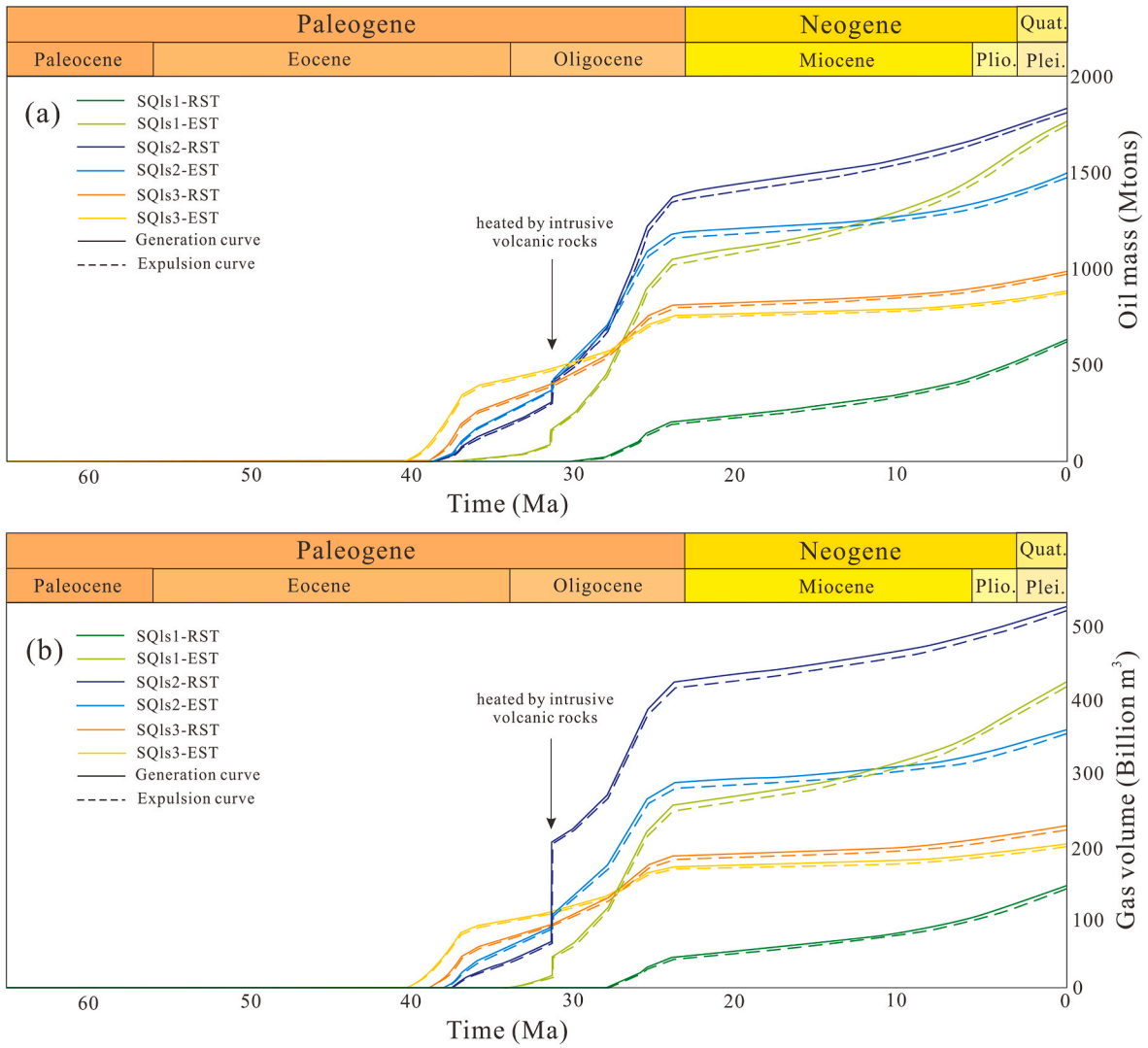

Fig. 19. Hydrocarbon generation and expulsion mass in different system tracts with geological time.

we can infer that most of the hydrocarbons generated by the effective source rocks are expelled due to the complex fracture system and the repeated superimposed carrier layers and source beds.

5.3. Implication for hydrocarbon exploration

This study presents a quantitative re-evaluation of the effective source rocks and hydrocarbon resources potential of the Fushan Depression using a practical 3D geological modeling approach. We have utilized comprehensive data, including logging curves, geochemical data, and seismic surveys, to ensure the results are both rational and scientifically sound. The distribution of effective oil and gas source rocks, as well as proven hydrocarbon reservoirs, is presented in Figs. 20 and 21, respectively. A correlation is observed between reservoir location and effective source rock distribution. According to previous studies, the Liushagang Formation vertically displays a double-layered structure, the upper and lower, characterized by the normal faults and antithetic normal faults, respectively, separated by the thick mudstone layer of SQls2 and rigid igneous rocks, forming two complete petroleum systems (Wang et al., 2014). The oil reservoirs in the lower tectonic layer are primarily located in the slope zone (the Meitai, Hongguang, and Bailian areas), supplied by the effective source rocks of SQls3-EST, SQls3-RST, and SQls2-EST. These reservoirs are capped by the thick mudstone layer of SQls2-RST and tightly surround the effective source kitchen (Fig. 20a–c). Oil migrates laterally along the high permeability sand bodies within the formation (Fig. 20a–c). In contrast, hydrocarbon accumulation in the upper tectonic layer is mainly concentrated in the central sag zone (the Yong'a and Huachang areas) and the fault-slope zone (the Chaoyang area), owing to the abundant presence of effective source rocks from SQls2-RST and SQls1 (Fig. 20d–f). Oil mainly migrates longitudinally along the faults (Fig. 20d–f). However, the hydrocarbon source rocks in the slope zone are almost immature. The northeastern Fushan Depression is characterized by a high concentration of effective gas source rocks, resulting in the presence of a few natural gas reservoirs (Fig. 21). In summary, the distribution of hydrocarbon accumulations is primarily controlled by the occurrence of these effective source rocks, which suggests favorable prospects for hydrocarbon exploration. These findings establish a geological foundation for further research on oil-source correlation, petroleum charging direction and distance, and drilling deployment. Additionally, the 3D stratigraphic model developed in this study is suitable for numerical simulation of petroleum migration and accumulation.

Unconventional oil and gas reservoirs, including in-source lithologic and frackable shale reservoirs, are increasingly attracting prospectors, prompting them to expedite the exploration process. However, accurately determining the distribution of effective source rocks is critical for finding these reservoirs. To this end, the authors recommend a 3D geological modeling approach to source rock evaluation, which

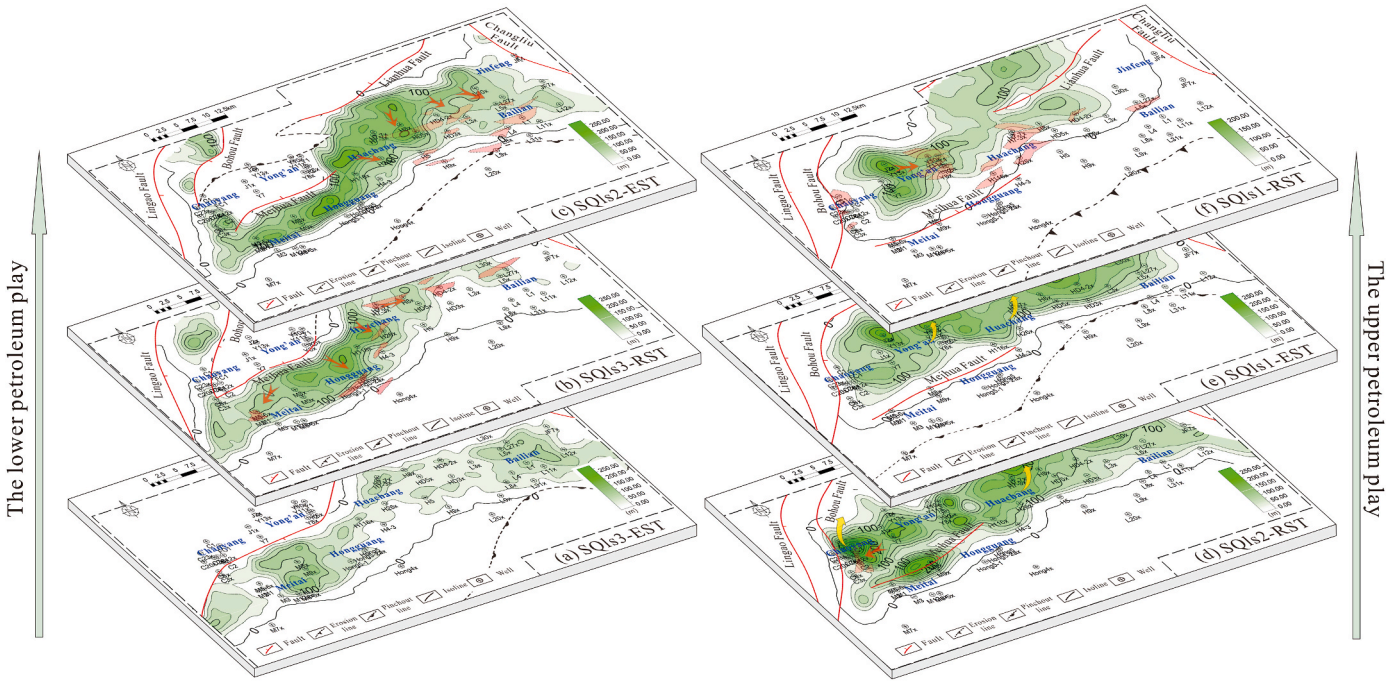

Fig. 20. Distribution of effective oil source rocks and proven oil reservoirs within the sequence stratigraphic framework. The red arrows indicate migration of hydrocarbons through high permeability sand bodies within the formation, while the yellow arrows indicate longitudinal migration along the fault.

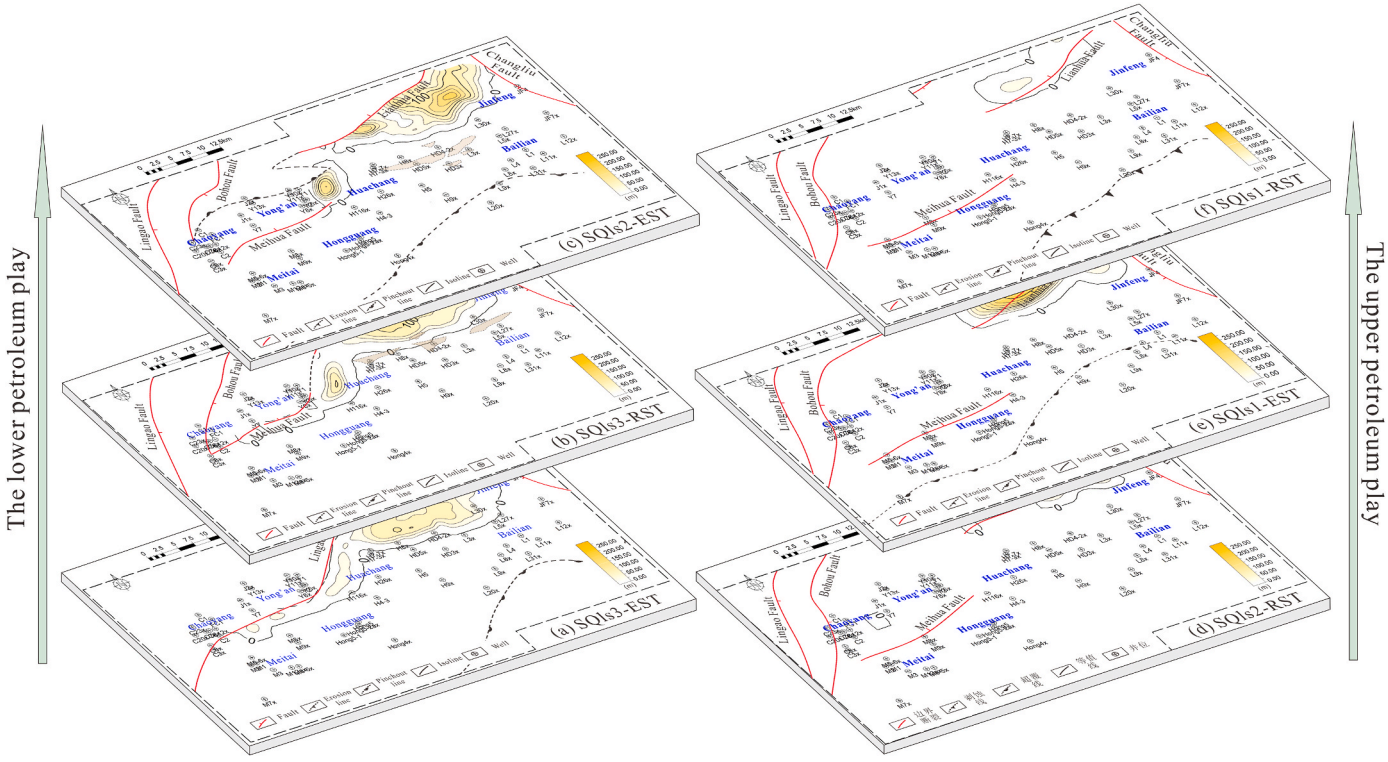

Fig. 21. Distribution of effective gas source rocks and proven gas reservoirs within the sequence stratigraphic framework.

complements geochemical experimental data by precisely depicting the location of effective hydrocarbon source rocks in space. As a result, the central Huangtong Sag (specifically the Yong'an area) is considered a promising area for unconventional resources, as the thickness of effective source rocks exceeds 600 m. This study can serve as a reference for future investigations on lacustrine source rocks in other petroleum-bearing basins.

5.4. The strengths and limitations of the workflow

The workflow presented in this paper offers three advantages and deviations when compared to prior literature. Firstly, instead of utilizing formations or members as the fundamental evaluation units, we place emphasis on the classification and assessment of lacustrine source rocks based on sedimentary facies. This approach stems from the observation

that source rocks within the same sedimentary environment exhibit similar geochemical characteristics, thus enabling a more comprehensive comprehension of oil-source correlations. Moreover, the spatial distribution of sedimentary facies within the sequence stratigraphic framework demonstrates a certain degree of predictability. Consequently, this method allows for the prediction of source rock subdivisions and their corresponding geochemical properties. Secondly, prior to predictions based on geophysics and mathematics, it is imperative to analyze the patterns of organic matter accumulation in various types of source rocks. This analysis provides geological constraints that enhance the accuracy of the results obtained. Thirdly, while previous studies on three-dimensional geological modeling predominantly focused on reservoirs and sand bodies, there has been limited quantitative research on source rocks, including their precise locations and volumes. In our proposed workflow, we advocate for the detailed modeling and quantitative characterization of effective source rocks. This is particularly significant in lacustrine basins where source rocks exhibit strong heterogeneity. Furthermore, these source rocks possess the potential to serve as unconventional reservoirs, necessitating accurate positioning and quantification.

It is worth noting that the discussion of three sequences together in this study is motivated by their overall similarity in paleoclimate and paleoproductivity, with sedimentation acting as the primary controlling factor for differential organic matter accumulation (Li et al., 2020; Zeng et al., 2022a). However, when extrapolating to other lacustrine basins, it may be necessary to have separate discussions if significant geological events such as climate shifts or volcanic eruptions occur between different sequences.

6. Conclusion

In conclusion, the identification and quantification of effective source rocks are crucial for locating hydrocarbon exploration objectives and optimizing well deployment. Conventional methods for investigating effective source rocks have limitations in providing accurate and precise information, particularly in lacustrine basins with high complexity and heterogeneity. In this study, we demonstrate through geochemical analysis that the TOC content of hydrocarbon source rocks follows a normal distribution in different sedimentary facies, suggesting a strong correlation between sedimentary facies and geochemical properties. We present a 3D geological modeling approach for predicting lacustrine effective source rocks and their hydrocarbon resource potential based on facies-controlled modeling that integrates geophysical techniques, geological theory, and geochemical data to overcome limitations in sample quantity and location. Compared to previous literature, this approach offers several notable advancements. Firstly, it incorporates a sedimentary facies-based classification and evaluation of source rocks, enhancing the accuracy of characterization. Secondly, mathematical modeling is constrained by considering organic enrichment patterns, ensuring more reliable predictions. Lastly, the approach emphasizes the three-dimensional modeling of effective source rocks, moving beyond the conventional focus solely on reservoirs. These improvements collectively contribute to a more comprehensive and robust methodology. The Fushan Depression, a Cenozoic lacustrine rift basin in the South China Sea, is used as a case study to demonstrate the effectiveness of this approach. The evaluation results show that the number of effective hydrocarbon source rocks in the Fushan Depression is far less than previously estimated and point out favorable areas for unconventional resources, thus improving oil and gas resource assessments and sustainable exploration. This approach has the potential to be applied in other lacustrine basins and greatly benefit the petroleum and natural gas industry.

Declaration of interest statement

The authors declare that they have no known competing financial interests or personal relationships that could have appeared to influence the work reported in this paper.

Data availability

Data will be made available on request.

Acknowledgments

This study was funded by the Hainan Fushan Oilfield Exploration and Development Company (2021-HNYJ-010). The authors are very grateful to ChatGPT for polishing and improving the language of this paper.

References

Abdullah, E.A., Abdelmaksoud, A., Hassan, M.A., 2022. Application of 3D static modelling in reservoir characterization: a case study from the qishn Formation in sharyoof oil field, masila basin, Yemen. Acta Geologica Sinica-English Edition 96 (1), 348–368.

Abdelmaksoud, A., Radwan, A.A., 2022. Integrating 3D seismic interpretation, well log analysis and static modelling for characterizing the Late Miocene reservoir, Ngatoro area, New Zealand. Geomechanics and Geophysics for Geo-Energy and Geo-Resources 8 (2), 63.

Alabert, F.G., Massonnat, G.J., 1990. Heterogeneity in a complex turbiditic reservoir: stochastic modelling of facies and petrophysical variability. In: SPE Annual Technical Conference and Exhibition. https://doi.org/10.2118/20604-MS. OnePetro.

Ali, A.M., Radwan, A.E., Abd El-Gawad, E.A., Abdel-Latief, A.A., 2022. 3D integrated structural, facies and petrophysical static modeling approach for complex sandstone reservoirs: a case study from the coniacian–santonian matulla formation, july Oilfield, gulf of suez, Egypt. Nat. Resour. Res. 31, 385–413. https://doi.org/10.1007/s11053-021-09980-9.

Allen, P.A., Allen, J.R., 2015. Basin Analysis: Principles and Application to Petroleum Play Assessment. John Wiley & Sons.

Al-Mudhafar, W.J., 2017. Geostatistical lithofacies modeling of the upper sandstone member/Zubair formation in south Rumaila oil field, Iraq. Arabian J. Geosci. 10, 1–14.

Aziz, H.A., Enrique, S.R., Calvo, J.P., Hilgen, F.J., Krijgsman, W., 2003. Palaeoenvironmental reconstruction of a middle Miocene alluvial fan to cyclic shallow lacustrine depositional system in the Calatayud Basin (NE Spain). Sedimentology 50 (2), 211–236.

Bordenave, M.L., Espitalié, J., Leplat, P., Oudin, J.L., Brouck, M.L.V.D., 1993. Screening techniques for source rock evaluation. In: Bordenave, M.L. (Ed.), Applied Petroleum Geochemistry. Editions Technip, Paris, pp. 218–278.

Bruce, P., Huppert, H., 1990. Solidification and melting along dykes by the laminar flow of basaltic magma. In: Ryan, M.P. (Ed.), Magma Transport and Storage. John Willey & Sons Ltd., pp. 87–101

Burnham, A.K., 1989. A Simple Kinetic Model of Petroleum Formation and Cracking. Lawrence Livermore National Lab., CA (USA).

Chen, S., Gan, H., Shi, Y., Zhao, Y., Wang, X., 2015. Geochemical features and geologic significance of source rocks in Fushan sag , Beibuwan basin. Petroleum Geology and Recovery Efficiency 22 (1), 14–19+25 (in Chinese with English abstract).

Chen, L., Gan, H., Zhu, C., Tian, J., 2002. Study on subsidence history of weixinan depression in Beibuwan Basin. Journal of Xinjiang Petroleum Institute 14 (4), 12–17 (in Chinese with English abstract).

Diab, A.I., Sanuade, O., Radwan, A.E., 2023. An integrated source rock potential, sequence stratigraphy, and petroleum geology of (Agbada-Akata) sediment succession, Niger delta: application of well logs aided by 3D seismic and basin modeling. J. Pet. Explor. Prod. Technol. 13 (1), 237–257.

Fertl, W., Chilingar, G., 1988. Total organic carbon content determined from well logs. SPE Form. Evaluation 3 (2), 407–419.

Friedmann, J.D., Olhoeft, G.R., Johnson, G.R., Frank, D., 1981. Heat content and thermal energy of the June dacite dome in relation to total energy yield. In: Lipman, P.W., Mullineaux, D.R. (Eds.), The 1980 Eruptions of Mount St. Helens. US Geological Survey Professional Paper 1250, pp. 557–568.

Gan, H., Wang, H., Shi, Y., Ma, Q., Liu, E., Yan, D., Pan, Z., 2020. Geochemical characteristics and genetic origin of crude oil in the fushansag, Beibuwan Basin, south China sea. Mar. Petrol. Geol. 112, 104114.

Hakimi, M.H., Abass, A.N., Lashin, A., Gharib, A.F., Radwan, A.E., Rahim, A., Ahmed, A., Asiwaju, L., Afify, W.E., 2022. Geochemical investigation and basin modelling of the Al renk shale formation in the Melut Basin, south Sudan: implications for estimation of thermogenic gas generation potential. Mar. Petrol. Geol. 146, 105926.

Hakimi, M.H., Lotfy, N.M., El Nady, M.M., Makled, W.A., Ramadan, F.S., Rahim, A., Talha Qadri, S.M., Lashin, A., Radwan, A.E., Mousa, D.A., 2023. Characterization of lower cretaceous organic-rich shales from the kom ombo basin, Egypt: implications for conventional oil generation. J. Asian Earth Sci. 241, 105459.

Hunt, J.M., 1979. Petroleum Geochemistry and Geology, first ed. W.H. Freeman and Company, New York, pp. 261–350.

Hunt, J.M., 1996. Petroleum Geochemistry and Geology, second ed. W.H. Freeman and Company, New York, p. 743.

Huo, Q., Zeng, H., Zhang, X., Fu, L., 2012. An evaluation diagram of effective source rocks in the first member of Qingshankou Formation in northern Songliao Basin and its implication. Acta Pet. Sin. 33 (3), 379–384 (in Chinese with English abstract).
Journel, A.G., Alabert, F.G., 1990. New method for reservoir mapping. J. Petrol. Technol. 42 (2), 212–218.
Kassem, A.A., Raafat, A., Radwan, A.E., El Nahas, S., Kędzierski, M., Zakaria, A., 2022. Paleoenvironment, sequence stratigraphy and source rock potentiality of the Cenomanian-Turonian boundary sediments of Southern Tethys. Mar. Petrol. Geol. 139, 105624.
Khattab, M.A., Radwan, A.E., El-Anbaawy, M.I., Mansour, M.H., El-Tehiwy, A.A., 2023. Three-dimensional structural modelling of structurally complex hydrocarbon reservoir in October Oil Field, Gulf of Suez, Egypt. Geol. J. https://doi.org/10.1002/gj.4748.
Lai, H., Li, M., Liu, J., Mao, F., Wang, Z., Liu, W., Yang, L., 2020a. Source rock assessment within a sequence stratigraphic framework of the Yogou Formation in the Termit Basin, Niger. Geol. J. 55 (4), 2473–2494.
Lai, H., Li, M., Liu, J., Mao, F., Liu, J., Xiao, H., Tang, Y., Shi, S., 2020b. Source rock types, distribution and their hydrocarbon generative potential within the Paleogene Sokor-1 and LV formations in Termit Basin, Niger. Energy Explor. Exploit. 38 (6), 2143–2168.
Lai, H., Li, M., Jian, X., Wang, L., Liu, J., Wang, G., Liu, P., Dai, J., 2020c. An integrated sequence stratigraphic–geochemical investigation of the Jurassic source rocks in the North Yellow Sea Basin, eastern China. AAPG (Am. Assoc. Pet. Geol.) Bull. 104 (10), 2145–2171.
Li, J., Wang, R., Qin, J., Qiu, K., 2020. Paleogene-Neogene micropaleontological records of the Weixinan Depression, Beibuwan Basin and their paleoenvironmental significance. Mar. Geol. Quat. Geol. 40 (2), 29–36. https://doi.org/10.16562/j.cnki.0256-1492.2019010901 (in Chinese with English abstract).
Li, Y., Deng, H., Tian, W., Cheng, Y., Zhang, Y., 2006. Application of impedance-constrained logging data in reservoir facies modeling. Petrol. Explor. Dev. 33 (5), 569–571.
Li, Y., Lin, S., Wang, H., Luo, D., 2017. Depositional setting analysis using seismic sedimentology: example from the Paleogene Liushagang sequence in the Fushan depression, South China Sea. Geodesy and Geodynamics 8, 347–355.
Li, Y., Wang, H., Liu, E., Liao, Y., Lin, Z., Ma, Q., 2014. Distribution regularities and control factors for reservoir formation within sequence stratigraphic framework in Fushan Sag, Beibuwan Basin. J. Cent. S. Univ. 45 (5), 1542–1554 (in Chinese with English abstract).
Li, M., Wang, T., Liu, J., Lu, H., Wu, W., Gao, L., 2008. Occurrence and origin of carbon dioxide in the fushan depression, Beibuwan Basin, south China sea. Mar. Petrol. Geol. 25, 500–513.
Liao, F., Ma, Q., Sun, X., Cheng, G., Zeng, W., Lu, Z., Shi, Y., Liu, D., 2015. Study of lithologic reservoir of paleogene Liushagang Formation in fushan depression of beibu bay basin. China Petroleum Exploration 20 (2), 43–50 (in Chinese with English abstract).
Liu, Y., Harding, A., Abriel, W., Strebelle, S., 2004. Multiple-point simulation integrating wells, three-dimensional seismic data, and geology. AAPG Bull. 88 (7), 905–921.
Liu, X., Liu, G., Song, Z., Jiang, W., Wang, N., 2022. The paleo-sedimentary environment and formation mechanism of the source rocks in shahejie formation, qikou sag, bohai bay basin. Nat. Gas Geosci. 33 (12), 2019–2042 (in Chinese with English abstract).
Liu, E., Wang, H., Li, Y., Leonard, N., Feng, Y., Pan, S., Xia, C., 2015. Relative role of accommodation zones in controlling stratal architectural variability and facies distribution: insights from the Fushan Depression, South China Sea. Mar. Petrol. Geol. 68, 219–239.
Liu, E., Wang, H., Li, Y., Zhou, W., Leonard, N., Lin, Z., Ma, Q., 2014. Sedimentary characteristics and tectonic setting of sublacustrine fans in a half-graben rift depression, Beibuwan Basin, South China Sea. Mar. Petrol. Geol. 52, 9–21.
Liu, E., Wang, H., Uysal, I.T., Zhao, J., Wang, X., Feng, Y., Pan, S., 2017. Paleogene igneous intrusion and its effect on thermal maturity of organic-rich mudstones in the Beibuwan Basin, South China Sea. Mar. Petrol. Geol. 86, 733–750.
Løseth, H., Wensaas, L., Gading, M., Duffaut, K., Springer, M., 2011. Can hydrocarbon source rocks be identified on seismic data? Geology 39 (12), 1167–1170.
Ma, Q., Zhao, S., Liao, Y., Lin, Z., 2012. Sequence architectures of paleogene Liushagang Formation and its significance in fushan sag of the Beibuwan Basin. Earth Sci. J. China Univ. Geosci. 37 (4), 667–678 (in Chinese with English abstract).
Magara, K., 1976. Thickness of removed sedimentary rocks,paleopore pressure,and paleotemperature,southwestern part of Western Canada basin. AAPG Bull. ,60, 554–566.
Magoon, L.B., 2004. Petroleum system: nature's distribution system for oil and gas. Encyclopedia of Energy 823–836. https://doi.org/10.1016/b0-12-176480-x/00251-5.
Mahmoud, A.A.A., Elkatatny, S., Mahmoud, M., Abouelresh, M., Abdulraheem, A., Ali, A., 2017. Determination of the total organic carbon (TOC) based on conventional well logs using artificial neural network. Int. J. Coal Geol. 179, 72–80.
Makled, W.A., Mostafa, T.F., Mousa, D.A., Abdou, A.A., 2018. Source rock evaluation and sequence stratigraphic model based on the palynofacies and geochemical analysis of the subsurface Devonian rocks in the Western Desert, Egypt. Mar. Petrol. Geol. 89, 560–584.
Mansour, A., Gentzis, T., Tahoun, S.S., Ahmed, M.S., Wagreich, M., Carvajal-Ortiz, H., Neumann, J., Radwan, A.E., 2023. Paleoenvironmental, paleoclimatic, and organic matter assessment of the hybrid Kharita Formation (Albian) in the Abu Gharadig Basin, Egypt: integration between palynology, organic petrography, and organic geochemistry. Mar. Petrol. Geol. 148, 106072.
Monreal, F.R., Villar, H.J., Baudino, R., Delpino, D., Zencich, S., 2009. Modeling an atypical petroleum system: a case study of hydrocarbon generation, migration and accumulation related to igneous intrusions in the Neuquen Basin, Argentina. Mar. Petrol. Geol. 26, 590–605.
Mort, H., Jacquat, O., Adatte, T., Steinmann, P., Föllmi, K., Matera, V., Berner, Z., Stüben, D., 2007. The Cenomanian/Turonian anoxic event at the Bonarelli Level in Italy and Spain: enhanced productivity and/or better preservation. Cretac. Res. 28 (4), 597–612.
Ogiesba, O., Hammes, U., 2014. Seismic-attribute identification of brittle and TOC-rich zones within the eagle ford shale, dimmit county, south Texas. J. Pet. Explor. Prod. Technol. 4 (2), 133–151.
Othman, R., Arouri, K.R., Ward, C.R., Mckirdy, D.M., 2001. Oil generation by igneous intrusions in the northern Gunnedah Basin, Australia. Org. Geochem. 32 (10), 1219–1232.
Pang, X.Q., 1995. Theory and Application of Hydrocarbon Expulsion Threshold. Petroleum Industry Press, Beijing, China, p. 270.
Pang, X., Li, Q., Chen, J., Li, M., Pang, H., 2014. Recovery method of original TOC and its application in source rocks at high mature - over mature stage in deep petroliferous basins. J. Palaeogeogr. 16 (6), 769–789.
Pang, X., Li, M., Li, S., Jin, Z., 2005. Geochemistry of petroleum systems in the Niuzhuang south slope of Bohai Bay basin. Part 3. Estimating hydrocarbon expulsion from the Shahejie Formation. Org. Geochem. 36 (4), 497–510.
Passey, Q., Creaney, S., Kulla, J., Moretti, F., Stroud, J., 1990. A practical model for organic richness from porosity and resistivity logs. AAPG Bull. 74, 1777–1794.
Pedersen, T.F., Calvert, S.E., 1990. Anoxia vs. Productivity: what controls the formation of organic-carbon-rich sediments and sedimentary rocks. AAPG Bull. 74 (4), 454–466.
Peters, K.E., 1986. Guidelines for evaluating petroleum source rock using programmed pyrolysis. AAPG Bull. 70, 318–329.
Peters, K.E., Walters, C.C., Mankiewicz, P.J., 2006. Evaluation of kinetic uncertainty in numerical models of petroleum generation. AAPG (Am. Assoc. Pet. Geol.) Bull. 90 (3), 387–403.
Peters, K.E., Kacewicz, M., Curry, D.J., 2012. An overview of basin and petroleum system modeling: definitions and concepts. In: Peters, K.E., Curry, D.J., Kacewicz, M. (Eds.), Basin Modeling: New Horizons in Research and Applications, vol. 4. AAPGHedberg Series, pp. 1–16.
Peters, K.E., Snedden, J.W., Sulaeman, A., Sarg, J.F., Enrico, R.J., 2000. A new geochemical-sequence stratigraphic model for the mahakam delta and makassar slope, kalimantan, Indonesia. AAPG Bull. 84 (1), 12–44.
Qin, J., 2005. The Source Rock in China. Science Press, Beijing, pp. 1–37.
Radwan, A.A., Abdelwahhab, M.A., Nabawy, B.S., Mahfouz, K.H., Ahmed, M.S., 2022. Facies analysis-constrained geophysical 3D-static reservoir modeling of Cenomanian units in the Aghar Oilfield (Western Desert, Egypt): insights into paleoenvironment and petroleum geology of fluviomarine systems. Mar. Petrol. Geol. 136, 105436.
Ribes, C., Kergaravat, C., Crumeyrolle, P., Lopez, M., Bonnel, C., Poisson, A., Kavak, K.S., Callot, J.P., Ringenbach, J.C., 2015. Factors controlling stratal pattern and facies distribution of fluvio-lacustrine sedimentation in the Sivas mini-basins, Oligocene (Turkey). Basin Res. 29, 596–621.
Ruggieri, R., Trippetta, F., Cassola, T., Petracchini, L., 2022. Basin modeling constrains source rock position and dimension in the Burano-Bolognano petroleum system (Central Italy). J. Asian Earth Sci. 240, 105436.
Sageman, B.B., Murphy, A.E., Werne, J.P., Straeten, C.A.V., Hollander, D.J., Lyons, T.W., 2003. A tale of shales: the relative roles of production, decomposition, and dilution in the accumulation of organic-rich strata, Middle–Upper Devonian, Appalachian basin. Chem. Geol. 195 (1–4), 229–273.
Sahoo, T.R., Funnell, R.H., Brennan, S.W., Sykes, R., Thrasher, G.P., Adam, L., Lawrence, M.J.F., Kellett, R.L., Ma, X., 2021. Delineation of coaly source rock distribution and prediction of organic richness from integrated analysis of seismic and well data. Mar. Petrol. Geol. 125, 104873.
Schmoker, J., 1979. Determination of organic content of Appalachian Devonian shales from formation-density logs. AAPG Bull. 63 (9), 1504–1509.
Seifert, D., Jensen, J.L., 1999. Using sequential indicator simulation as a tool in reservoir description: issues and uncertainties. Math. Geol. 31, 527–550.
Seifert, D., Jensen, J.L., 2000. Object and pixel-based reservoir modeling of a braided fluvial reservoir. Math. Geol. 32, 581–603.
Sheikh, H.E., Faris, M., Shaker, F., Kumral, M., 2016. Mineralogy and source rock evaluation of the marine Oligo-Miocene sediments in some wells in the Nile Delta and North Sinai, Egypt. J. Afr. Earth Sci. 118, 163–173.
Simoneit, B., Brenner, S., Peters, K.E., Kaplan, I.R., 1978. Thermal alteration of Cretaceous black shale by basaltic intrusions in the Eastern Atlantic. Nature 273, 501–504.
Sweeney, J., Burnham, A.K., 1990. Evaluation of a simple model of vitrinite reflectance based on chemical kinetics. AAPG Bull. 74, 1559–1570.
Tawfik, A.Y., Ondrak, R., Winterleitner, G., Mutti, M., 2022. Source rock evaluation and petroleum system modeling of the east beni suef basin, north eastern desert, Egypt. J. Afr. Earth Sci. 193, 104575.
Thiry, M., 1989. Geochemical evolution and paleoenvironments of the eocene continental deposits in the Paris Basin. Palaeogeogr. Palaeoclimatol. Palaeoecol. 70 (1–3), 0–163.
Tissot, B.P., Welte, D.H., 1984. Petroleum Formation and Occurrence. Springer-Verlag, Berlin.
Wang, G., Huang, C., Liu, E., Li, Y., Pan, S., 2014. Characteristics of slope-breaks and its control on sedimentation and hydrocarbon accumulation of Liushagang Formation in gentle slope of south Fushan sag. J. Cent. S. Univ. 45 (5), 1531–1541 (in Chinese with English abstract).
Wang, X., Lu, Z., Li, M., Guo, H., Zhu, Z., Li, X., Yang, C., Zeng, B., Wang, F., Ran, Z., 2022. Petroleum charging history of the paleogene sandstone reservoirs in the Huangtong sag of the fushan depression, south China sea. Energies 15, 1374.

Wang, H., Wu, W., Chen, T., Dong, X., Wang, G., 2019. An improved neural network for TOC, S1 and S2 estimation based on conventional well logs. J. Pet. Sci. Eng. 176, 664–678.

Wygrala, B., 1989. Integrated Study of an Oil Field in the Southern Po Basin, Northern Italy. Kernforschungsanlage Jülich GmbH. Verlag Jülich, Zentralbiliothek, p. 328.

Zeinalzadeh, A., Moussavi-Harami, R., Mahboubi, A., Sajjadian, V.A., 2015. Basin and petroleum system modeling of the Cretaceous and Jurassic source rocks of the gas and oil reservoirs in Darquain field, south west Iran. Mar. Petrol. Geol. 26, 419–426.

Zeng, B., Li, M., Wang, N., Shi, Y., Wang, F., Wang, X., 2022a. Geochemistry and heterogeneous accumulation of organic matter in lacustrine basins: a case study of the Eocene Liushagang Formation in the Fushan Depression, South China Sea. Petrol. Sci. 19 (6), 2533–2548.

Zeng, B., Li, M., Wang, X., Wang, F., Gong, C., Lai, J., Shi, Y., 2022b. Source rock evaluation within a sequence stratigraphic framework of the palaeogene Liushagang Formation in the fushan depression, south China sea. Geol. J. 57 (6), 2409–2427.

Zeng, B., Li, M., Zhu, J., Wang, X., Shi, Y., Zhu, Z., Guo, H., Wang, F., 2021. Selective methods of TOC content estimation for organic-rich interbedded mudstone source rocks. J. Nat. Gas Sci. Eng. 93 (5), 104064.

Zhang, J., He, J., Gong, X., Zhang, X., Huang, W., 2012. Petroleum system, oil and gas migration and accumulation in fushan depression, Beibuwan Basin of the South China sea. Marine Geology Frontiers 28 (1), 30–37 (in Chinese with English abstract).

Zhang, S., Shao, L., Song, J., Liu, D., Chen, G., Ren, C., 2008. Application of facies-controlled modeling technology to the fault-block A11 in A'Nan Oilfield. Petrol. Explor. Dev. 35 (3), 355–361.

Zheng, D., Pang, X., Ma, X., Li, C., Zheng, T., Zhou, L., 2019. Hydrocarbon generation and expulsion characteristics of the source rocks in the third member of the Upper Triassic Xujiahe Formation and its effect on conventional and unconventional hydrocarbon resource potential in the Sichuan Basin. Mar. Petrol. Geol. 109, 175–192.

Zhu, C., Jiang, F., Zhang, P., Hu, T., Liu, Y., Xu, T., Zhang, Y., Deng, Q., Zhou, Y., Xiong, H., Song, Z., 2021. Identification of effective source rocks in different sedimentary environments and evaluation of hydrocarbon resources potential: a case study of paleogene source rocks in the Dongpu Depression, Bohai Bay Basin. J. Pet. Sci. Eng. 201, 108477.